Variational theory of preroughening

Santi Prestipino
Istituto Nazionale per la Fisica della Materia, Trieste, Italy

Erio Tosatti*
Istituto Nazionale per la Fisica della Materia, Trieste, Italy;
International School for Advanced Studies, Trieste, Italy;
and International Centre for Theoretical Physics, Trieste, Italy
(Received 1 June 1998)

Saito's variational mean-field theory of roughening [Y. Saito, Z. Phys B **32**, 75 (1978)] is generalized to include preroughening. The starting point is a sine-Gordon Hamiltonian with a cosine parameter changing sign at a temperature T_{PR}. This theory accounts for a number of known features of preroughening from solid-on-solid lattice models, including logarithmic divergence of the average interface width as a function of the system size and continuous crystal growth at T_{PR}. When T_{PR} reduces to one quarter of the roughening temperature or less, preroughening becomes first order. We also consider adsorption over an attractive substrate. Using our variational theory, we calculate adsorption isotherms. They show a reentrant layering pattern, which connects well with observations for noble gases adsorbed on graphite. [S0163-1829(98)05543-X]

I. INTRODUCTION

Since the introduction of the preroughening (PR) transition of crystal surfaces by Den Nijs and Rommelse,[1] a number of theoretical approaches,[2,3] and of numerical studies of solid-on-solid lattice models[4,5] as well as of step models,[6] have clarified the behavior at this unusual phase transition. Here we list a number of well-established results. The average surface height jumps from roughly integer in the smooth, or ordered flat phase, below PR, to roughly half-odd integer values in the disordered flat (DOF) phase, above PR. The average square height difference diverges logarithmically approaching the (isolated) PR transition temperature T_{PR}. The surface-specific heat has a nonuniversal singularity at PR. Crystal growth is continuous exactly at T_{PR}, and is layer by layer, with a finite activation energy, both below and above T_{PR}. Transitions between half-integer coverages are expected in adsorption over an attractive substrate at temperatures between T_{PR} and T_R.

Clearcut experimental evidence of a surface PR transition on e.g., metal surfaces, has apparently not yet been identified, possibly due to slow kinetics or to associated phase-separation phenomena between DOF phases with neighboring heights.[7] However, reentrant layering has been observed in adsorption isotherms for several rare gases on graphite,[8,9] and has been attributed to PR.[10] Preroughening is also found in realistic Lennard-Jones surface simulations,[11] where it appears to mark the onset of surface melting.

Surprisingly enough, there is as yet no mean-field treatment of PR for comparison with this wealth of theoretical, experimental, and simulation evidence. In the present paper, Saito's treatment of the roughening transition,[12] which employs a variational, mean-field approach to study surface equilibrium, supplemented by a Langevin equation for growth and dynamics, is extended to PR. The extension is obtained simply by allowing, phenomenologically, the cosine parameter of the sine-Gordon trial Hamiltonian to become negative at a temperature T_{PR} (the PR temperature) below T_R.[1] In this way, we are able to reproduce, qualitatively in all cases, exactly in some cases, the known phenomenology related to PR and to the DOF phase.

This paper is organized as follows. After an initial review in Sec. II of known results which will be needed later, we present in Sec. III our model and the variational derivation of its static properties, and in Sec. IV a numerical exemplification of the equilibrium phase diagram in a variety of conditions. Then, in Sec. V, we consider growth, by analyzing the dynamical response to a chemical-potential driving force. In Sec. VI, we consider adsorption on a substrate, and derive adsorption isotherms, which are in their turn exemplified numerically in Sec. VII. Finally, we present a short discussion and concluding remarks in Sec. VIII.

II. BRIEF REVIEW

Crystal surfaces are often described within the solid-on-solid (SOS) approximation, characterized by a single two-dimensional lattice height variable h_i, separating the interior of the crystal and the outside vacuum.[13] The simplest nontrivial surface model of this kind is the discrete Gaussian (DG) model

$$\mathcal{H}_{DG}=\frac{J}{2}\sum_{i,\delta}(h_i-h_{i+\delta})^2, \tag{2.1}$$

with integer heights, $h_i=0,\pm 1,\pm 2,\ldots$, and where the sum is restricted to nearest-neighbor pairs of lattice sites (to be specific, from now on we consider a square lattice). In Eq. (2.1), $J>0$ is the surface stiffness, and the heights are expressed in units of the vertical lattice spacing. The DG model is well known[14] to undergo a roughening transition of the Kosterlitz-Thouless type at $T_R=4/\pi$ (hereafter, all temperatures in units of J/k_B).

A closely related model is the sine-Gordon model

$$\mathcal{H}_{sG}=\frac{J}{2}\sum_{i,\delta}(h_i-h_{i+\delta})^2+y_2\sum_i[1-\cos(2\pi h_i)], \tag{2.2}$$

with continuous heights and $y_2>0$. This model is in the same universality class as the DG model,[15] but is easier to handle analytically, being a field theory. A number of well-known results have been obtained from renormalization-group treatments of Hamiltonian (2.2).[16] Summarizing, the roughening transition is of infinite order, i.e., the surface free energy shows an essential singularity at T_R of the kind $f\sim\exp\{-A|T-T_R|^{-1/2}\}$; below T_R the surface is flat, meaning that the average surface height $\bar{h}=\langle(1/N)\Sigma_i h_i\rangle$ is well defined, and the average square height difference approaches a number at large distance. Precisely, one finds

$$\langle(h_i-h_j)^2\rangle\sim 2\langle(h_i-\bar{h})^2\rangle+B\exp\left(-\frac{|\mathbf{r}_i-\mathbf{r}_j|}{\xi}\right), \tag{2.3}$$

with a correlation length ξ diverging, as the roughening temperature is approached from below, as $\xi\sim\exp\{C(T_R-T)^{-1/2}\}$.

Two decades ago, when renormalization-group methods were in their infancy, Saito devised a variational theory of the roughening transition which, even if partly failing to reproduce the precise behavior at T_R, nonetheless had the advantage of capturing the main features of the roughening phenomenon, being in addition transparent and straightforward.[12] In this approximation, the transition temperature is exact, and the infinite-order character of the transition is accounted for. More detailed, the form of the free-energy singularity is slightly wrong, since one finds $-\ln f_{\rm sing}\sim\ln\xi\sim(T_R-T)^{-1}$, instead of $(T_R-T)^{-1/2}$, for $T\lesssim T_R$. In dynamics, Saito's theory correctly describes the jump from activated to continuous surface growth, reproducing the results of the more rigorous theory.[17,18]

Given its simplicity and effectiveness, it is desirable to generalize this kind of variational theory so as to embody the additional possibility of preroughening. The usual way to introduce PR in a SOS Hamiltonian is to add some interaction between the surface steps. When parallel steps (i.e., steps of same sign) repel each other more than antiparallel steps, PR will generally occur at some temperature $T_{PR}<T_R$. Between T_{PR} and T_R, the surface is in a DOF state, characterized by a mesh of up-down correlated steps, leading to a half-coverage of the topmost surface layer, that is to a half-odd-integer average surface height. One particular case of antiparallel-step attraction, leading to PR, is realized on some surfaces which have a tendency toward missing-row surface reconstructions. When realized, as for example in Au(110), these reconstructions consist of a statically ordered array of up-down steps, already leading to half-coverage at $T=0$. In this case, the PR transition and the deconstruction transition coincide.

III. MODEL AND ITS VARIATIONAL TREATMENT

Phenomenologically, preroughening can be mimicked by means of a sine-Gordon Hamiltonian, where the cosine parameter sign can change.[10] For example, it suffices to modify the sine-Gordon model slightly as follows:

$$\mathcal{H}=\frac{J}{2}\sum_{i,\delta}(h_i-h_{i+\delta})^2+y_2\sum_i[1-\cos(2\pi h_i)]+y_4\sum_i[1-\cos(4\pi h_i)], \tag{3.1}$$

by keeping $y_4>0$ constant, and by allowing y_2 to change sign at a temperature T_{PR}. To be specific, let us assume a linear T dependence

$$y_2(T)=C(T_{PR}-T), \tag{3.2}$$

with $C>0$. Equations (3.1) and (3.2) can be considered as a coarse-grained approximation to the true microscopic Hamiltonian, in that C, T_{PR}, and y_4 parametrize for a specific SOS lattice model exhibiting the same thermodynamic properties. An explicit mapping between a restricted SOS model with parallel-step repulsion and a sine-Gordon-type free energy with y_2 changing sign at some temperature T_{PR} has been recently produced using a plaquette mean-field theory.[19]

The mechanism inducing PR in the Hamiltonian (3.1) is simply explained. When $y_4>0$ and the temperature is not too high, the $\cos(4\pi h)$ term pins the surface height indifferently at either integer or half-integer values. However, as y_2 becomes negative, i.e., upon crossing T_{PR}, the average surface height jumps from integer to half-integer, thus provoking PR of the surface.

Variationally, we can now approximate the exact, unknown free energy of $\mathcal{H}$ by means of that generated by a simpler, soluble Hamiltonian:

$$\mathcal{H}_0=\frac{J}{2}\sum_{i,\delta}(h_i-h_{i+\delta})^2+J\xi^{-2}\sum_i(h_i-\bar{h})^2, \tag{3.3}$$

with continuous heights. Here the average height $\bar{h}$ and the correlation length ξ are variational parameters (both are assumed to be dimensionless, measuring numbers of vertical and horizontal lattice spacings, respectively). As in other mean-field theories, the variational principle is provided by the Bogolubov thermodynamic inequality[20]

$$F\leq F_0+\langle\mathcal{H}-\mathcal{H}_0\rangle_0, \tag{3.4}$$

where F_0 is the free energy relative to $\mathcal{H}_0$ and $\langle\cdots\rangle_0$ is an average over the ensemble specified by $\mathcal{H}_0$. At each temperature, choosing such $\bar{h}$ and ξ that minimize $F^*=F_0+\langle\mathcal{H}-\mathcal{H}_0\rangle_0$ will give the optimal free energy per site as

$$f_{\rm best}(T)=\frac{1}{N}\min_{\{\bar{h},\xi\}}F^*(T;\bar{h},\xi). \tag{3.5}$$

At the same time, we shall identify the stable surface phase according to the following ''dictionary'': $\xi^{-2}=0$, rough phase; half-integer $\bar{h}$ and $\xi^{-2}>0$, DOF phase; integer $\bar{h}$ and $\xi^{-2}>0$, ordered flat phase.

Details of the calculation, which is straightforward, can be found in Appendix A. In the rough phase, the variational free energy reads:

$$\beta f^*(\xi^{-2}=0)\equiv\frac{\beta F^*(\xi^{-2}=0)}{N}$$
$$=-\frac{\pi}{8}\ln\frac{\pi}{\beta J}+\frac{\pi}{8}[\ln(\pi^2)-1]+\beta(y_2+y_4), \tag{3.6}$$

with $\beta J=1/T$. Equation (3.6) gives the optimal free energy whenever $\Delta f^*(\xi^{-2})\equiv f^*(\xi^{-2})-f^*(0)$ is minimum at $\xi^{-2}=0$ (i.e., strictly positive). It is shown in detail in Appendix A that

$$\beta\Delta f^*=\frac{\pi}{8}\ln(1+(\pi\xi)^{-2})$$
$$-\beta y_2\cos(2\pi\bar{h})[1+(\pi\xi)^2]^{-(\pi/4\beta J)}$$
$$-\beta y_4\cos(4\pi\bar{h})[1+(\pi\xi)^2]^{-(\pi/\beta J)}, \tag{3.7}$$

with

$$\sin(2\pi\bar{h})=0 \tag{3.8}$$

and

$$J\xi^{-2}=2\pi^2 y_2\cos(2\pi\bar{h})[1+(\pi\xi)^2]^{-(\pi/4\beta J)}$$
$$+8\pi^2 y_4\cos(4\pi\bar{h})[1+(\pi\xi)^2]^{-(\pi/\beta J)} \tag{3.9}$$

as necessary conditions in order that Δf^* be extremal.

We have two classes of solutions for $\bar{h}$ from Eq. (3.8): integers $[\cos(2\pi\bar{h})=1]$ and half-integers $[\cos(2\pi\bar{h})=-1]$. Given Eq. (3.2), the ordered flat phase (integer $\bar{h}$) is more stable than the DOF phase (half-integer $\bar{h}$) when $T<T_{PR}$, and the opposite for $T>T_{PR}$. Hence, PR occurs precisely at T_{PR}. Moreover, $y_2\cos(2\pi\bar{h})=|y_2|$, $\cos(4\pi\bar{h})=1$, and Eqs. (3.7) and (3.9) simplify to

$$\beta\Delta f^*=\frac{\pi}{8}\ln[1+(\pi\xi)^{-2}]-\beta|y_2|[1+(\pi\xi)^2]^{-(\pi/4\beta J)}$$
$$-\beta y_4[1+(\pi\xi)^2]^{-(\pi/\beta J)}, \tag{3.10}$$

$$J\xi^{-2}=2\pi^2|y_2|[1+(\pi\xi)^2]^{-(\pi/4\beta J)}$$
$$+8\pi^2 y_4[1+(\pi\xi)^2]^{-(\pi/\beta J)}. \tag{3.11}$$

Equation (3.11) is still too complex to solve analytically. However, we can at least analyze what happens near T_R and T_{PR} where, as can be readily shown, there are divergent ξ solutions to Eq. (3.11).

When $\xi\gg 1$, Eq. (3.11) becomes

$$2\frac{|y_2|}{J}(\pi\xi)^{2[1-(T/T_R)]}+8\frac{y_4}{J}(\pi\xi)^{2[1-(4T/T_R)]}\simeq 1, \tag{3.12}$$

where $T_R=4/\pi$. If $T\lesssim T_R$, then $(\pi\xi)^{2[1-(4T/T_R)]}\ll 1$ can be ignored, and we obtain

$$\xi\simeq\frac{1}{\pi}\exp\left[\frac{\frac{1}{2}\ln\left(\frac{J}{2|y_2(T)|}\right)}{1-\frac{T}{T_R}}\right], \tag{3.13}$$

which diverges to $+\infty$ as $T\to T_R^-$, provided $J/[2|y_2(T_R)|]>1$, or $C<C^*(T_{PR})$, where

$$C^*(T)=\frac{J}{2(T_R-T)}. \tag{3.14}$$

When y_2 is a positive constant, Eq. (3.13) describes the behavior near the roughening transition.[12] Hence T_R is recognized as the roughening transition temperature. As already noted, ξ in Eq. (3.13) diverges with the wrong power of 1 instead of $\frac{1}{2}$. When $C>C^*(T_{PR})$, there is no divergent solution to Eq. (3.11) for $T\lesssim T_R$, and ξ remains finite at T_R, which therefore is no longer the roughening temperature. As we shall see below, the true roughening is first order and takes place at $T_R^*>T_R$.

Now consider $T\simeq T_{PR}$, when $T_R/4<T_{PR}<T_R$. In this case, a divergent ξ must be such that

$$\frac{2C|T-T_{PR}|}{J}(\pi\xi)^{2[1-(T_{PR}/T_R)]}\simeq 1, \tag{3.15}$$

leading in turn to

$$\xi\simeq\frac{1}{\pi}\left(\frac{2C|T-T_{PR}|}{J}\right)^{-1/[2(1-T_{PR}/T_R)]}\sim|T-T_{PR}|^{-\nu}, \tag{3.16}$$

with

$$\nu=\frac{T_R}{2(T_R-T_{PR})}. \tag{3.17}$$

Hence, ξ diverges as a power law at the PR transition. Note, in particular, the absence of y_4 from both Eqs. (3.13) and (3.16). For this reason, y_4 is irrelevant to the critical behavior of the extended sine-Gordon model, at least so long as $T_{PR}>T_R/4$.

According to Eq. (3.16), the best $\mathcal{H}_0$ at T_{PR} is a Gaussian model, i.e., the same as for the regular rough phase. Thus, for a finite surface of lateral size N at $T=T_{PR}$ we have $\langle\delta h^2\rangle\sim(1/4\pi K_c)\ln N$, with a roughness parameter $K_c=\pi\nu/(4\nu-2)$ (Ref. 1) equal to

$$K_c=\frac{\pi}{4}\frac{T_R}{T_{PR}}. \tag{3.18}$$

We note that the absolute surface roughness exactly at PR, as measured by the prefactor of $\ln N$, namely, $1/4\pi K_c$, is just a fraction T_{PR}/T_R of that at roughening, and will thus be proportionally lower, the lower T_{PR} is with respect to T_R.

Given Eq. (3.17), the specific-heat exponent is obtained from the hyperscaling relation:

$$\alpha=2-2\nu=\frac{T_R-2T_{PR}}{T_R-T_{PR}}. \tag{3.19}$$

α is negative for $T_R/2<T_{PR}<T_R$, varying from $-\infty$ as $T_{PR}\to T_R^-$, to $+\frac{2}{3}$ as $T_{PR}\to(T_R/4)^+$. Nonuniversal critical

exponents have indeed been predicted for PR.[1] Equations (3.17) and (3.19) indicate an approximate connection between them and the transition temperatures.

Another important quantity is the PR order parameter, defined (in the smooth phase) as

$$P=\left|\left\langle \frac{1}{N}\sum_i (-1)^{h_i}\right\rangle_0\right|. \tag{3.20}$$

After noting that $(-1)^{h_i}=e^{\pi i h_i}$, we can use Eq. (A21) to obtain $P=[1+(\pi\xi)^2]^{-(\pi/16\beta J)}$. In particular, for $T\lesssim T_{PR}$ we have $P\sim(T_{PR}-T)^{\beta_P}$, with

$$\beta_P=\frac{T_{PR}}{4(T_R-T_{PR})}. \tag{3.21}$$

This result is consistent with Gaussian criticality at PR, which would in fact predict the same β_P, i.e., $(\pi/4)/(4K_c-\pi)$.[4]

When $T=T_{PR}=T_R/4$, Eq. (3.11) becomes

$$J\xi(T_{PR})^{-2}=\frac{8\pi^2 y_4}{1+\pi^2\xi(T_{PR})^2}, \tag{3.22}$$

which gives a finite ξ solution, $\xi(T_{PR})=1/\pi[(8y_4/J)-1]^{-1/2}$, when $y_4>J/8$. Otherwise, the only solution to Eq. (3.22) for $y_4<J/8$ is $\xi(T_{PR})=+\infty$.

When $T_{PR}<T_R/4$, there is no ξ divergence from Eq. (3.11) near T_{PR}. In fact, ξ shows a cusplike singularity at T_{PR}, and PR becomes first-order (Sec. IV). $\xi(T_{PR})$ can still diverge exponentially as $T_{PR}\to(T_R/4)^-$:

$$\xi(T_{PR})\simeq\frac{1}{\pi}\exp\left[\frac{\frac{1}{2}\ln\left(\frac{J}{8y_4}\right)}{1-\frac{4T_{PR}}{T_R}}\right], \tag{3.23}$$

but only if $y_4<J/8$. Otherwise, $\xi(T_{PR})$ remains finite as $T_{PR}\to(T_R/4)^-$.

Finally, when $y_4=0$ and $T\simeq T_{PR}$, the correlation length behaves like Eq. (3.16), which is now valid for any $T_{PR}<T_R$. This means that the change from critical to first-order behavior at $T_{PR}=T_R/4$ only occurs when $y_4>0$.

We now evaluate $\langle(h_m-\overline{h})^2\rangle_0$ for $h_m=(1/N)\Sigma_i h_i$, in order to check how sharply is $\overline{h}$ defined at equilibrium. Using a similar device to Eq. (A10), we obtain:

$$\langle(h_m-\overline{h})^2\rangle_0=\frac{1}{N^2}\sum_{i,j}\langle(h_i-\overline{h})(h_j-\overline{h})\rangle_0=\frac{\xi^2}{2N\beta J}, \tag{3.24}$$

which is to be considered as a good definition whenever ξ is finite, i.e., away from criticality.

Once $\xi(T)$ is given, the average surface width follows directly from the general relationship [after Eqs. (A20) and (A27)]

$$\langle\delta h^2\rangle\equiv\frac{1}{N}\left\langle\sum_i (h_i-\overline{h})^2\right\rangle_0=\frac{1}{8\pi\beta J}\ln[1+(\pi\xi)^2]. \tag{3.25}$$

Using the above results, we can derive the behavior of $\langle\delta h^2\rangle$ near criticality. For $T\lesssim T_R$ and $C<C^*(T_{PR})$, we have

$$\langle\delta h^2\rangle\simeq\frac{\frac{T}{2\pi^2}\ln\left(\frac{J}{2|y_2(T)|}\right)}{T_R-T} \tag{3.26}$$

(power-law singularity at roughening), whereas

$$\langle\delta h^2\rangle\simeq-\frac{T}{2\pi^2(T_R-T_{PR})}\ln\left(\frac{2C|T-T_{PR}|}{J}\right) \tag{3.27}$$

near T_{PR}, when $T_R/4<T_{PR}<T_R$ (logarithmic singularity at PR).

Finally, we analyze the free-energy singularity at the two transitions, as follows from Eq. (3.10) and from the above ξ solutions. When $T>T_R$ and $\xi^{-2}\ll 1$, one has

$$\beta\Delta f^*\simeq\frac{1}{8\pi}\xi^{-2}, \tag{3.28}$$

and $\xi^{-2}=0$ is a local minimum of Δf^*, *but* not necessarily the lowest. On the other hand, when $T<T_R$, $\xi^{-2}=0$ provides a local maximum for Δf^* (i.e., zero). When $T\lesssim T_R$ and $\xi^{-2}\ll 1$, it follows that

$$\Delta f_{\rm best}\simeq-\frac{J}{2}\left(1-\frac{T}{T_R}\right)\exp\left[-\frac{\ln\left(\frac{J}{2|y_2(T)|}\right)}{1-\frac{T}{T_R}}\right], \tag{3.29}$$

as long as $C<C^*(T_{PR})$. $\Delta f_{\rm best}$ then shows an essential singularity at T_R, but of the wrong type, as already commented. Near T_{PR}, ξ only diverges for $T_{PR}>T_R/4$, in which case we have

$$\Delta f_{\rm best}\simeq-\frac{J}{2}\left(1-\frac{T_{PR}}{T_R}\right)\left(\frac{2C|T-T_{PR}|}{J}\right)^{\omega}, \tag{3.30}$$

with

$$\omega=2\nu=\frac{T_R}{T_R-T_{PR}}. \tag{3.31}$$

We remark that the specific heat, proportional to $\partial^2\Delta f_{\rm best}/\partial T^2$, behaves like $|T-T_{PR}|^{\omega-2}$ near PR; hence $\alpha=2-\omega$, a result consistent with hyperscaling [Eq. (3.19)].

All of the above indicates that PR only exists as a continuous transition when $T_{PR}>T_R/4$. We now move to the numerical analysis and see whether the solutions found really provide in each case the absolute minimum free energy.

IV. NUMERICAL RESULTS: FREE SURFACE

In order to make these results more tangible, we now present a numerical exemplification. In Fig. 1, we plot $\xi(T)$ for $T_{PR}=0.5$, $C=0.5J$, and $y_4=0.1J$ (other values of y_4 were not found to affect substantially the ξ profile in Fig. 1). Note that $C<C^*(0.5)$. Looking at Fig. 1, we see that the correlation length distinctly diverges at PR as a power law [cf. Eq. (3.16)], signalling a second-order phase transition (with $\alpha=0.353$). When approaching T_R from below, ξ di-

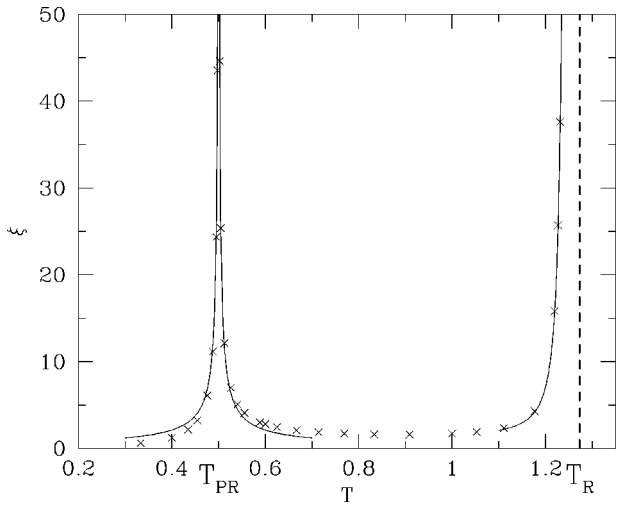

FIG. 1. Variational correlation length $\xi(T)$ when $T_{PR}=0.5$, $C=0.5J$, and $y_4=0.1J$. With these parameters, $C<C^*(0.5)$. The correlation length is $+\infty$ beyond $T_R=4/\pi$. Continuous lines give the behavior near the two transition points [cf. Eqs. (3.13) and (3.16)]. We note from this picture that the critical region extends well beyond a small neighborhood of the two transition points.

verges even faster [cf. Eq. (3.13)], while remaining infinite above T_R. We also verified that $\Delta f_{\rm best}$ has the expected behavior near T_{PR} [cf. Eqs. (3.30) and (3.31)] and near T_R [cf. Eq. (3.29)]. The scenario represented in Fig. 1 is thought to be generic, as far as $T_{PR}>T_R/4$. In this case, our variational theory gives a reasonable account of the behavior of the restricted SOS model of Ref. 4. There PR is signalled by the switch from integer to half-integer mean height, and also by the logarithmic broadening of the surface upon increasing its lateral size.

In Fig. 2, we plot $\xi(T)$ for $T_{PR}=0.25$, $C=0.5J$, in the

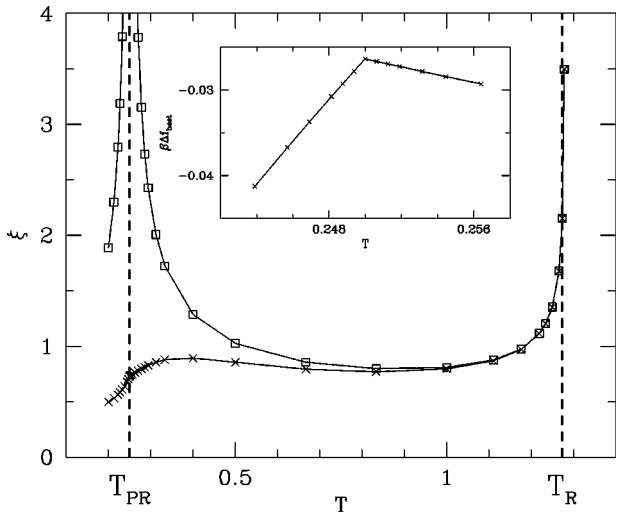

FIG. 2. Variational correlation length $\xi(T)$ when $T_{PR}=0.25$, $C=0.5J$, for $y_4=0$ ($\square$) and $y_4=0.1J$ ($\times$). With these parameters, $C>C^*(0.25)$, and the correlation length remains finite at T_R, which in this case is not the roughening temperature. There is instead a first-order roughening transition at $T_R^*=1.2785>T_R$. The PR transition is critical for $y_4=0$, but first order for $y_4=0.1J$ (in the inset, the free energy $\beta\Delta f_{\rm best}$ for $y_4=0.1J$ shows a cusplike singularity at T_{PR}).

two cases $y_4=0$ and $y_4=0.1J$. Now $C>C^*(0.25)$. Although the ξ profile for $y_4=0$ is quite similar to Fig. 1, a cusp develops at T_{PR} when $y_4=0.1J$ ($\Delta f_{\rm best}$ behaves likewise, signalling a first-order PR transition; see the inset of Fig. 2). In both cases, ξ undergoes an infinite jump at $T=T_R^*=1.2785$, slightly above $T_R=1.2732$ (first-order roughening transition at T_R^*). This behavior should be representative of the case $T_{PR}<T_R/4$ in general. We verified that $T_R^*(T_{PR})$ moves to the left, until T_R is reached, as $C\to C^*(0.25)^+$ (the same effect is also obtained by keeping $C=0.5J$ fixed and increasing T_{PR} up to $T_R-(J/2C)=T_R-1$). This indicates that, although $\xi^{-2}=0$ is a local minimum of Δf^* when $T>T_R$, it does not represent the absolute minimum as far as $T<T_R^*$, since the branch providing the minimum Δf^* for $T<T_R$ still gives the stable ξ solution until $T=T_R^*$.

Then, we numerically check the sensitivity of ξ to y_4, since there appeared [cf. Eq. (3.23)] a change of behavior at $y_4=J/8$. Taking $C=0.5J$, we separately consider $y_4<J/8$ and $y_4>J/8$. When $y_4<J/8$, $\xi\to+\infty$ at PR provided $T_{PR}>T_R/4$, while remaining finite when $T_{PR}<T_R/4$. In this case, $\xi(T_{PR})$ grows to infinity as $T_{PR}\to(T_R/4)^-$ according to Eq. (3.23). When $y_4>J/8$, we find that $\xi\to+\infty$ at PR only if $T_{PR}>T_{PR}^*(y_4)$, where T_{PR}^* is a slightly larger temperature than $T_R/4$. Otherwise, for $T_{PR}<T_{PR}^*(y_4)$, ξ remains finite at PR, which is then first order. In fact, although a free-energy minimum is present along the branch providing a divergent ξ for any $T_{PR}>T_R/4$, this minimum is not the absolute minimum until $T_{PR}=T_{PR}^*(y_4)$. The interval between $T_R/4$ and T_{PR}^* is very narrow, and grows only slowly as y_4 grows. We find $T_{PR}^*(0.126J)=0.318\,61$ ($\xi^{-2}=0.022$), $T_{PR}^*(0.13J)=0.320\,25$ ($\xi^{-2}=0.124$), and $T_{PR}^*(0.15J)=0.331\,11$ ($\xi^{-2}=0.804$). When $T_{PR}>T_{PR}^*(y_4)$, we also find two further transitions at temperatures not very far from T_{PR}; one inside the smooth phase (at $T=T_1<T_{PR}$), and the other inside the DOF phase (at $T=T_2>T_{PR}$). They are first-order transitions with a finite jump in the correlation length. These transitions appear as soon as T_{PR} overcomes $T_{PR}^*(y_4)$, but they disappear soon after, at two different values of T_{PR}. We quote some results relative to $y_4=0.15$: the transition at T_1 is no longer present for $T_{PR}>0.337$, whereas the one at T_2 has already disappeared at $T_{PR}=0.333$; furthermore, for $T_{PR}=0.3325$, we have $T_1=0.3320$ and $T_2=0.3346$. These prewettinglike transitions have not been described before, to our knowledge. Their true physical relevance is at present unclear. Besides the evidence of a $T_R^*(T_{PR})>T_R$ [when $C>C^*(T_{PR})$], the only other anomaly found in the theoretical scenario presented above is the existence of a $T_{PR}^*(y_4)>T_R/4$ (when $y_4>J/8$).

In conclusion, we find that the PR transition in the extended sine-Gordon model is, according to our variational calculation, continuous for $T_{PR}>T_R/4$ and first order for $T_{PR}<T_R/4$. In terms of K_c [Eq. (3.18)], second-order PR will occur for $\pi/4<K_c<\pi$, while first-order PR will be observed for $K_c>\pi$. The π threshold for continuous PR is also found in the extended BCSOS model of Ref. 21. Moreover, the above results on the nature of the PR transition in the extended sine-Gordon model are in excellent agreement with renormalization-group theory.[3] This is gratifying, even if

somewhat surprising, considering the nominal mean-field nature of our theory. In fact, our trial Hamiltonian (3.3) embodies nontrivial correlations between the heights, and this explains why the present theory is so informative.

V. GROWTH: LANGEVIN DYNAMICS

In this section, we analyze the near-equilibrium dynamics of the extended sine-Gordon model [Eq. (3.1)]. We consider the Langevin growth equation

$$\frac{\mathrm{d}h_i}{\mathrm{d}t}=-\frac{\beta}{\tau}\frac{\delta\mathcal{H}}{\delta h_i}+\zeta_i, \tag{5.1}$$

where a term $-\Delta\mu\Sigma_i h_i$ (with $\Delta\mu>0$) has been absorbed into $\mathcal{H}$ to induce crystal growth. In Eq. (5.1), τ is the relaxation time, and $\{\zeta_i(t)\}$ is a Gaussian white noise:

$$\langle\zeta_i(t)\rangle_\zeta=0,\quad \langle\zeta_i(t)\zeta_j(t')\rangle_\zeta=\frac{2}{\tau}\delta_{ij}\delta(t-t'), \tag{5.2}$$

where the averages are over a Gaussian distribution $P_\zeta[\{\zeta_i(t)\}]\propto\exp[-(\tau/4)\int \mathrm{d}t\Sigma_i\zeta_i(t)^2]$.

A first, limited, result is the exact solution of the Langevin equation for the mean surface height $h_m=(1/N)\Sigma_i h_i$, when $T=T_{PR}$ and $y_4=0$. In this case, Eq. (5.1) becomes

$$\frac{dh_m}{dt}=\frac{\beta\Delta\mu}{\tau}+\zeta_m, \tag{5.3}$$

with $\zeta_m=(1/N)\Sigma_i\zeta_i$, $\langle\zeta_m(t)\rangle_\zeta=0$, and $\langle\zeta_m(t)\zeta_m(t')\rangle_\zeta=(2/N\tau)\delta(t-t')$. Integrating Eq. (5.3) and then averaging, we obtain

$$\langle[h_m(t)-h_m(0)]^2\rangle_\zeta=\left(\frac{\beta\Delta\mu}{\tau}t\right)^2+\frac{2}{N\tau}t. \tag{5.4}$$

At equilibrium, $\Delta\mu=0$, we find that the interface as a whole diffuses like a Brownian particle, with a diffusion coefficient $1/N\tau$ which is vanishingly small in the infinite-size limit.

Next, we move to the general case. As usual, Eq. (5.1) can be studied through the associated Fokker-Planck equation[22]

$$\frac{\partial P(\{h_i\},t)}{\partial t}=\frac{\beta}{\tau}\sum_i\ \frac{\delta}{\delta h_i}\left(P\frac{\delta\mathcal{H}}{\delta h_i}+\frac{1}{\beta}\frac{\delta P}{\delta h_i}\right) \tag{5.5}$$

for the height density function $P(\{h_i\},t)=\langle\Pi_i\delta[h_i-h_i(t,\{\zeta_i(t)\})]\rangle_\zeta$, where $h_i(t,\{\zeta_i(t)\})$ is the solution to the Langevin equation for a particular realization of the noise. Any noise average can be expressed as an ensemble average over the P distribution, according to:

$$\langle F[\{h_i(t,\{\zeta_i(t)\})\}]\rangle_\zeta=\left\langle\int\mathcal{D}h\Pi_i\delta[h_i-h_i(t,\{\zeta_i(t)\})]F(\{h_i\})\right\rangle_\zeta=\int\mathcal{D}h\langle\Pi_i\delta[h_i-h_i(t,\{\zeta_i(t)\})]\rangle_\zeta F(\{h_i\})\equiv\langle F(\{h_i\})\rangle_P. \tag{5.6}$$

It is shown in detail in Appendix B that, upon assuming a Gaussian for P, the average surface height $\bar{h}(t)$ and the pair correlation in momentum space $g(\mathbf{p},t)$ are found to obey the equations

$$\frac{\mathrm{d}\bar{h}(t)}{\mathrm{d}t}=\frac{\beta}{\tau}\left[\Delta\mu-2\pi y_2\sin(2\pi\bar{h}(t))\exp\left(-\frac{\pi^2}{N}\sum_{\mathbf{p}}\ g(\mathbf{p},t)^{-1}\right)-4\pi y_4\sin[4\pi\bar{h}(t)]\exp\left(-\frac{4\pi^2}{N}\sum_{\mathbf{p}}\ g(\mathbf{p},t)^{-1}\right)\right], \tag{5.7}$$

$$\frac{\mathrm{d}}{\mathrm{d}t}g(\mathbf{p},t)^{-1}=-\frac{4}{\tau}g(\mathbf{p},t)^{-1}\left[\lambda(\mathbf{p})-g(\mathbf{p},t)+2\pi^2\beta y_2\cos[2\pi\bar{h}(t)]\exp\left(-\frac{\pi^2}{N}\sum_{\mathbf{p}}\ g(\mathbf{p},t)^{-1}\right)\right.$$
$$\left.+8\pi^2\beta y_4\cos[4\pi\bar{h}(t)]\exp\left(-\frac{4\pi^2}{N}\sum_{\mathbf{p}}\ g(\mathbf{p},t)^{-1}\right)\right]. \tag{5.8}$$

Equations (5.7) and (5.8) form a set of coupled equations which appears hard to solve. As in Ref. 12, we decouple these two equations by neglecting the effect of a time-dependent $\bar{h}$ on the evolution of $g(\mathbf{p},t)$, which is then identified with the equilibrium $g(\mathbf{p})$ (quasistationary approximation). In this way, we wind up with:

$$\frac{\mathrm{d}\bar{h}(t)}{\mathrm{d}t}=\frac{\beta}{\tau}\{\Delta\mu-\mathrm{sgn}(y_2)\Delta\mu_c\sin[2\pi\bar{h}(t)]-\Delta\mu_c'\sin[4\pi\bar{h}(t)]\}, \tag{5.9}$$

where

$$\Delta\mu_c=2\pi|y_2|[1+(\pi\xi)^2]^{-(\pi/4\beta J)},\qquad \Delta\mu_c'=4\pi y_4[1+(\pi\xi)^2]^{-(\pi/\beta J)}. \tag{5.10}$$

The form of the solution critically depends upon $\Delta\mu_c$ and $\Delta\mu_c'$. A special case is when ξ is infinite (PR, when critical, and the rough phase). In this case, $\Delta\mu_c=\Delta\mu_c'=0$ and Eq. (5.9) is easily solved as $\bar{h}(t)=(\beta\Delta\mu/\tau)t$, which describes continuous growth. This is well known,[17,18] and also found in Monte Carlo simulations of restricted SOS models.[4,23]

The behavior of $\Delta\mu_c$ and $\Delta\mu_c'$, for $T\lesssim T_R$ and $C<C^*(T_{PR})$, is easily found to be:

$$\Delta\mu_c\simeq 2\pi|y_2|(\pi\xi)^{-2T/T_R},\quad \Delta\mu_c'=O(\Delta\mu_c^4). \tag{5.11}$$

$\Delta\mu_c$ is called the depinning field since the crystal does not grow for $\Delta\mu<\Delta\mu_c$ (see below). At first sight, it is puzzling that, according to Eq. (5.11), $\Delta\mu_c$ close to T_R appears to be set by the energy scale y_2 (the bare surface pinning potential) rather than J (the *renormalized* pinning potential), as it should be on physical grounds. For example, Nozières and Gallet[18] showed that the depinning field

$$\Delta\mu_c \sim \frac{\gamma a^2}{\xi^2}, \tag{5.12}$$

where γ is the renormalized surface stiffness at T_R, and a (here=1) is the step height. Since $\gamma a^2=\frac{\pi}{2}k_BT_R$,[18] which in turn equals $2J$, one has $\Delta\mu_c\sim 2J/\xi^2$. However, a simple algebraic manipulation [see Eq. (3.13)],

$$(\pi\xi)^{-(2T/T_R)} \simeq \left(\frac{J}{2|y_2|}\right)^{-T/(T_R-T)} \simeq \frac{J}{2|y_2|}(\pi\xi)^{-2}, \tag{5.13}$$

shows that

$$\Delta\mu_c \simeq \frac{J}{\pi\xi^2}, \tag{5.14}$$

that is, our result for $\Delta\mu_c$ below roughening is in fact in full agreement with Eq. (5.12), and is correctly controlled by J and not by y_2.

Next, let us consider what happens to the depinning field just below and just above T_{PR}. There are no previous results about this. For $T_{PR}>T_R/4$, PR is critical and we find from Eqs. (5.10) and (3.16):

$$\Delta\mu_c \sim |T-T_{PR}|^{\omega}, \quad \Delta\mu_c' \sim |T-T_{PR}|^{4T_{PR}/(T_R-T_{PR})}, \tag{5.15}$$

where $\omega=T_R/(T_R-T_{PR})$ is the same exponent as for the free energy [cf. Eq. (3.30)], and is typically much larger than 1. It follows that pinning of the flat surface to integer height values and that of the DOF surface to half-integer height values close to PR is much stronger in comparison with that found below roughening. A glance at Fig. 1, for example, shows that ξ^2 will grow large only very close to T_{PR}, which implies, via Eq. (5.14), that only there does $\Delta\mu_c$ truly become small.

Finally, we find that the role of $\Delta\mu_c'$ is irrelevant: since $4T_{PR}/(T_R-T_{PR})>\omega$ [cf. Eq. (3.31)], there exists a neighborhood of T_{PR} where $\Delta\mu_c' \ll \Delta\mu_c$, meaning that $\Delta\mu_c'$ can be neglected at least sufficiently near criticality.

We now wish to compute $\overline{h}(t)$. Equation (5.9) is exactly solvable when $y_4=0$.[12] We set $\overline{h}(0)=0$ and distinguish between a) $\Delta\mu>\Delta\mu_c$ and b) $\Delta\mu<\Delta\mu_c$. In case (a), we find

$$\overline{h}(t)=\frac{1}{\pi}\arctan\left[\frac{\mathrm{sgn}(y_2)\Delta\mu_c+D\,\tan\left(\pi\beta D\frac{t}{\tau}-\mathrm{sgn}(y_2)\arctan\frac{\Delta\mu_c}{D}\right)}{\Delta\mu}\right]+n, \tag{5.16}$$

for $(n-1)(\tau/\beta D)+t_0<t<n(\tau/\beta D)+t_0$, n integer, with $D=\sqrt{\Delta\mu^2-\Delta\mu_c^2}$ and $t_0=(\tau/\beta D)[\frac{1}{2}+(1/\pi)\mathrm{sgn}(y_2)\arctan(\Delta\mu_c/D)]$. $\overline{h}(t)$ is a stepwise increasing function of time with step period $\tau/\beta D$. The increase becomes linear as $\Delta\mu$ grows to infinity. $\overline{h}$ is never stationary; however, its rate of increase is minimum at $\overline{h}=\frac{1}{4}+k$, k integer, when $y_2>0$ (smooth phase); or at $\overline{h}=\frac{3}{4}+k$, k integer, when $y_2<0$ (DOF phase). This feature is different from results of restricted SOS simulations, where the staircase plateaus occur rather accurately at integer or half-integer numbers (when $T<T_{PR}$ or $T>T_{PR}$, respectively).[4,23]

Below the critical depinning field (case b), $\Delta\mu<\Delta\mu_c$, one finds

$$\overline{h}(t)=\frac{1}{\pi}\arctan\left[\frac{\mathrm{sgn}(y_2)\Delta\mu_c-D}{\Delta\mu}\,\frac{e^{2\pi\beta D(t/\tau)}-1}{e^{2\pi\beta D(t/\tau)}-\frac{\mathrm{sgn}(y_2)\Delta\mu_c-D}{\mathrm{sgn}(y_2)\Delta\mu_c+D}}\right], \tag{5.17}$$

with $D=\sqrt{\Delta\mu_c^2-\Delta\mu^2}$. When $y_2>0$ (flat surface), the denominator is always positive and $\overline{h}$ increases monotonically up to $1/\pi\ \arctan(\Delta\mu_c-D)/\Delta\mu$. When $y_2<0$ (DOF surface), the solution to Eq. (5.9) is again similar to that for $y_2>0$. However, as $\overline{h}$ crosses $\frac{1}{2}$ at $(\tau/2\pi\beta D)\ln[(\Delta\mu_c+D)/(\Delta\mu_c-D)]$, the right-hand side of Eq. (5.17) adds another 1, eventually leveling off at a value <1. Hence, in this regime there are no oscillations and the crystal does not grow (in reality, the growth mechanism would be nucleation, which is, however, beyond the scope of our theory). Hence $\Delta\mu_c$ really represents the threshold which the driving force must ultimately overcome in order to cause continuous crystal growth. Similar is the outcome of a renormalization-group treatment of the growth mode near roughening:[18] a sufficiently large $\Delta\mu$ is needed in order to observe continuous (i.e., substantial) growth for $T<T_R$, whereas an infinitesimal $\Delta\mu$ suffices for $T\geqslant T_R$.

The last point to discuss is what happens when including $\Delta\mu_c'$. It turns out that this factor has little influence on the evolution of $\overline{h}$ as compared to $\Delta\mu_c$ (some numerical results can be found in Fig. 3). As before, we ask what are the values of $\overline{h}$ when its slope is minimum. Alternatively, we

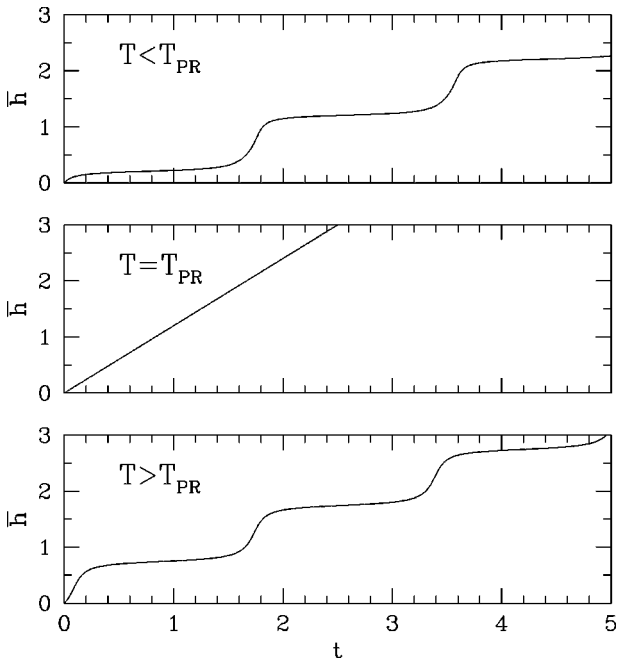

FIG. 3. Surface growth in our variational theory: average surface height $\overline{h}(t)$ as a function of time for $T_{PR}=0.5$, $C=0.5J$, and $y_4=0.2J$, at three different temperatures: top, $T<T_{PR}$ (smooth phase; the following parameters were used: $T^{-1}=2.2$, $\xi^{-2}=0.123$, $\Delta\mu=0.032J$, and $\tau=0.033$); center, $T=T_{PR}$ (we used $\Delta\mu=0.012J$ and $\tau=0.02$); and bottom, $T>T_{PR}$ (DOF phase; we used $T^{-1}=1.8$, $\xi^{-2}=0.062$, $\Delta\mu=0.02J$, $\tau=0.018$). The smooth jumps in the average height both below and above preroughening are indicative of layer-by-layer growth in the linear-response regime. Note, however, that the jumps do not occur between either integer (top) or half-integer values (bottom).

seek for $Z(\overline{h})=\mathrm{sgn}(y_2)\Delta\mu_c\sin(2\pi\overline{h})+\Delta\mu_c'\sin(4\pi\overline{h})$ being maximum. Obviously, we here consider only the growth regime, $\max Z(\overline{h})<\Delta\mu$. A simple analysis shows that when $\Delta\mu_c'<\Delta\mu_c/2$ there is a unique $Z(\overline{h})$ maximum at

$$\overline{h}=\frac{1}{2\pi}\arccos\left(\frac{-\Delta\mu_c+\sqrt{\Delta\mu_c^2+32\Delta\mu_c'^2}}{8\Delta\mu_c'}\right)+k, \tag{5.18}$$

k integer, for $y_2>0$; or at

$$\overline{h}=1-\frac{1}{2\pi}\arccos\left(\frac{\Delta\mu_c-\sqrt{\Delta\mu_c^2+32\Delta\mu_c'^2}}{8\Delta\mu_c'}\right)+k, \tag{5.19}$$

k integer, for $y_2<0$. When $\Delta\mu_c'\geqslant\Delta\mu_c/2$, another local maximum appears, but it never overcomes the first. Finally, as $\Delta\mu_c'$ increases, Eqs. (5.18) and (5.19) move from $\frac{1}{4}+k$ to $\frac{1}{8}+k$, and from $\frac{3}{4}+k$ to $\frac{5}{8}+k$, respectively. We note that these values differ from integers and half-integers typical of equilibrium and also of growth on SOS models,[4,23] while they are not inconsistent with the evidence provided by realistic Lennard-Jones simulations.[11]

VI. ADSORPTION ONTO AN ATTRACTIVE SUBSTRATE

The theory above is for a free surface. However, the main experimental claims of surface preroughening have been made for thin multilayer films of rare-gas solids adsorbed on attractive substrates. These data show that the film thickness, i.e., the average quantity of adsorbed matter, is, below the roughening temperature, a staircaselike function of chemical potential. More specifically, it is a function of the difference $\Delta\mu$ between the chemical potential of the bulk interface and that of the film (not to be confused with the quantity $\Delta\mu$ of Sec. V, which is just the opposite). Roughly, these layering jumps occur between integer layer numbers at low temperatures, and disappear due to roughening at high temperatures. In detail, however, a reentrant behavior was observed in Ar, for example: the jumps first disappear at about 82% of the melting temperature; then they reappear above this temperature, but this time between roughly half-integer layer numbers; finally they disappear for good at about 94% of the melting temperature, where roughening is known to take place.[8] Other subtler features in the layering phase diagram of Ar have also been reported, in the form of zigzagging heat-capacity peaks joining low- and high-temperature layering transition lines.[9] A very similar reentrant layering behavior has also been found recently in a grand-canonical Monte Carlo simulation for Lennard-Jones particles.[11]

Den Nijs first suggested that the reentrant first-order layering transitions should be indicative of PR of the bulk interface.[10] More recently, Weichman and Prasad provided a renormalization-group theory of adsorption which compares well with the experiments.[3] Here we show that our variational theory is capable of accounting in detail for this rich adsorption phase diagram. To this end, we follow earlier work by Weeks, who studied the standard case, without PR.[24] We use the extended sine-Gordon Hamiltonian (3.1), augmented by a term $\Sigma_i V(h_i)$ describing the influence of the substrate. The substrate potential mainly serves to define a mean film thickness, $h_0\sim\Delta\mu^{-1/3}$, diverging as $\Delta\mu$ goes to zero. This can be accounted for by using the Weeks prescription for the potential,

$$V(h)=\Delta\mu h+\frac{c}{2h^2}, \tag{6.1}$$

with $c>0$, and where the heights are zero at the substrate. The first term in Eq. (6.1) favors the gas phase with respect to the solid, and thus works against adsorption, whereas the second term describes van der Waals attraction by the substrate. Near its point of minimum, $h_0=(\Delta\mu/c)^{-1/3}$, $V(h)$ is approximated by

$$V(h_0)+\frac{1}{2}V''(h_0)(h-h_0)^2, \tag{6.2}$$

with $V''(h_0)\sim(\Delta\mu/c)^{4/3}$. For simplicity, we assume form (6.2) to be valid in general (the error made is small in the thick-film limit).

In the same spirit of Sec. III, we estimate the free energy of our model [Hamiltonian $\mathcal{H}+V(h)$] using the Bogolubov inequality, Eq. (3.4). We obtain

$$\frac{1}{N}\left\langle \sum_i V(h_i)\right\rangle_0 = V(h_0)+\frac{1}{2}V''(h_0)\left\langle \frac{1}{N}\sum_i (h_i-h_0)^2\right\rangle_0 = V(h_0)+\frac{1}{2}V''(h_0)(\overline{h}-h_0)^2+\frac{V''(h_0)}{16\pi\beta J}\ln[1+(\pi\xi)^2], \tag{6.3}$$

and then, using earlier results [see Eq. (3.7)], we arrive at the free-energy functional

$$\beta\Delta f^* = \beta V(h_0)+\frac{\beta}{2}V''(h_0)(\overline{h}-h_0)^2+\frac{V''(h_0)}{16\pi J}\ln[1+(\pi\xi)^2]+\frac{\pi}{8}\ln[1+(\pi\xi)^{-2}]$$
$$-\beta y_2\cos(2\pi\overline{h})[1+(\pi\xi)^2]^{-(\pi/4\beta J)}-\beta y_4\cos(4\pi\overline{h})[1+(\pi\xi)^2]^{-(\pi/\beta J)}, \tag{6.4}$$

with ξ and $\overline{h}$ being selected so as to minimize Δf^*. Necessary conditions for this are

$$V''(h_0)(\overline{h}-h_0)+2\pi\,\sin(2\pi\overline{h})[1+(\pi\xi)^2]^{-(\pi/4\beta J)}\{y_2+4y_4\cos(2\pi\overline{h})[1+(\pi\xi)^2]^{-(3\pi/4\beta J)}\}=0 \tag{6.5}$$

and

$$J\xi^{-2}=\frac{V''(h_0)}{2}+2\pi^2 y_2\cos(2\pi\overline{h})[1+(\pi\xi)^2]^{-(\pi/4\beta J)}+8\pi^2 y_4\cos(4\pi\overline{h})[1+(\pi\xi)^2]^{-(\pi/\beta J)}. \tag{6.6}$$

These equations must be solved numerically. When more than one solution is found, the such is chosen that provides the minimum $\Delta f_{\rm best}(T,\Delta\mu)$ of Δf^*.

In Sec. VII we solve Eqs. (6.4)–(6.6) numerically in a number of selected cases. However, one can even go beyond the quadratic approximation (6.2). For example, if we keep up to fourth-order terms in the expansion of $V(h)$ around h_0, then Eq. (6.4) must be modified as follows:

$$\beta\Delta f^* = \beta V(h_0)+\frac{\beta}{2}V''(h_0)(\overline{h}-h_0)^2+\frac{\beta}{6}V'''(h_0)(\overline{h}-h_0)^3+\frac{\beta}{24}V^{iv}(h_0)(\overline{h}-h_0)^4$$
$$+\frac{V''(h_0)+V'''(h_0)(\overline{h}-h_0)+\frac{1}{2}V^{iv}(h_0)(\overline{h}-h_0)^2}{16\pi J}\ln[1+(\pi\xi)^2]+\frac{V^{iv}(h_0)}{512\pi^2\beta J^2}\ln^2[1+(\pi\xi)^2]$$
$$+\frac{\pi}{8}\ln[1+(\pi\xi)^{-2}]-\beta y_2\cos(2\pi\overline{h})[1+(\pi\xi)^2]^{-(\pi/4\beta J)}-\beta y_4\cos(4\pi\overline{h})[1+(\pi\xi)^2]^{-(\pi/\beta J)}. \tag{6.7}$$

Equations (6.5) and (6.6) are then replaced by

$$V''(h_0)(\overline{h}-h_0)+\frac{V'''(h_0)}{2}(\overline{h}-h_0)^2+\frac{V^{iv}(h_0)}{6}(\overline{h}-h_0)^3+\frac{V'''(h_0)+V^{iv}(h_0)(\overline{h}-h_0)}{16\pi\beta J}\ln(1+(\pi\xi)^2)+2\pi\,\sin(2\pi\overline{h})$$
$$\times[1+(\pi\xi)^2]^{-(\pi/4\beta J)}\{y_2+4y_4\cos(2\pi\overline{h})[1+(\pi\xi)^2]^{-(3\pi/4\beta J)}\}=0 \tag{6.8}$$

and

$$J\xi^{-2}=\frac{1}{2}\left[V''(h_0)+V'''(h_0)(\overline{h}-h_0)+\frac{1}{2}V^{iv}(h_0)(\overline{h}-h_0)^2\right]+\frac{V^{iv}(h_0)}{32\pi\beta J}\ln[1+(\pi\xi)^2]$$
$$+2\pi^2 y_2\cos(2\pi\overline{h})[1+(\pi\xi)^2]^{-(\pi/4\beta J)}+8\pi^2 y_4\cos(4\pi\overline{h})[1+(\pi\xi)^2]^{-(\pi/\beta J)}, \tag{6.9}$$

respectively. We postpone a discussion of third- and fourth-order corrections to results obtained within the quadratic approximation until the end of Sec. VII.

VII. NUMERICAL RESULTS: ADSORBED FILM ON A SUBSTRATE

First we consider the case $T_{PR}>T_R/4$. To be specific, we take $T_{PR}=0.5$, $C=0.5J$, and $y_4=0.1J$ (see Fig. 1 for the bulk-interface behavior). We set $c=J$ in what follows. A typical low-temperature adsorption isotherm is plotted in Fig. 4 ($T=0.4$). Here we show both ξ and $\overline{h}$ as a function of h_0. Besides a less interesting behavior at large $\Delta\mu$, we see sharp jumps of the film height $\overline{h}$ between nearly integer values every time h_0 equals an integer-plus-one-half, and without any loss of continuity for $\Delta f_{\rm best}$. This is the film coun-

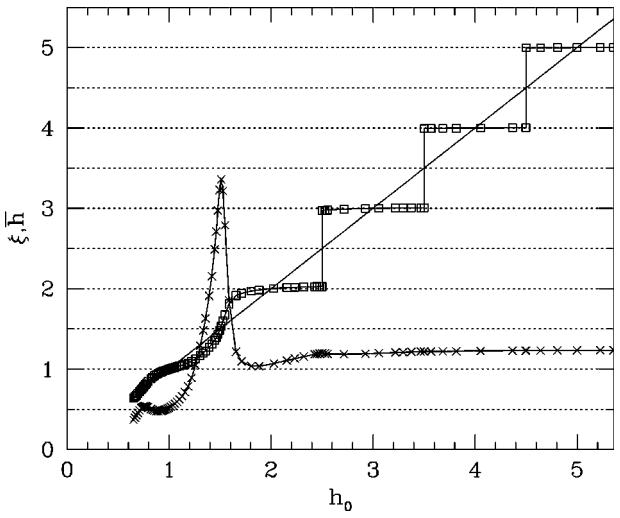

FIG. 4. Variational correlation length ξ ($\times$) and height $\bar{h}$ ($\square$), during growth, as a function of $h_0=(\Delta\mu/c)^{-1/3}$ (also drawn as a continuous line through the $\bar{h}$ data), along the adsorption isotherm $T=0.4$, for $T_{PR}=0.5$. Sharp jumps of $\bar{h}$ between integer values signal the crossing of first-order layering transition lines.

terpart of the bulk-interface smooth phase, whose degeneracy is removed by a nonzero $\Delta\mu$ which selects among pure states the one with the nearest height to h_0. At every $\bar{h}$ jump, a cusp is found for ξ, which becomes less and less sharp as h_0 grows, until ξ attains the bulk-interface value (1.2394 for $T=0.4$). Moreover, from Fig. 5 we see that jumps are also found in the numerical $\Delta\mu$ derivative of $\Delta f_{\rm best}$; this is not surprising, given that $(\partial\Delta f_{\rm best}/\partial\Delta\mu)_\beta$ is the variational estimate of the average film width (to be compared with $\bar{h}$ in Fig. 4) when the original $V(h)$ is used [Eq. (6.1)]. Starting from $h_0=1.5$, half-integer values of h_0 define first-order transition lines ending in noncritical points whose temperatures $T^{(1.5)},T^{(2.5)},T^{(3.5)},\ldots$ eventually converge to T_{PR} as a power law, $T_{PR}-T^{[n-(1/2)]}\sim n^{-p_1(T_{PR})}$, with $p_1(T_{PR})\simeq 2.510$.

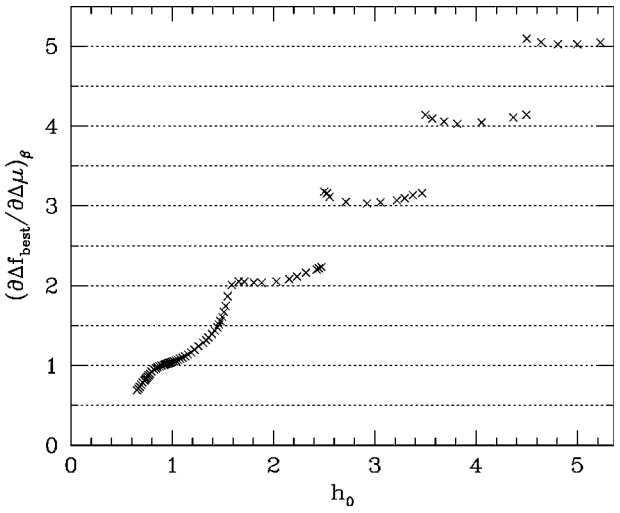

FIG. 5. Variational estimate of $\bar{h}$ through the $\Delta\mu$ derivative of $\Delta f_{\rm best}$, for $T=0.4$ and $T_{PR}=0.5$. The small discrepancies from Fig. 4 are due to the quadratic approximation of the substrate potential [cf. Eq. (6.2)].

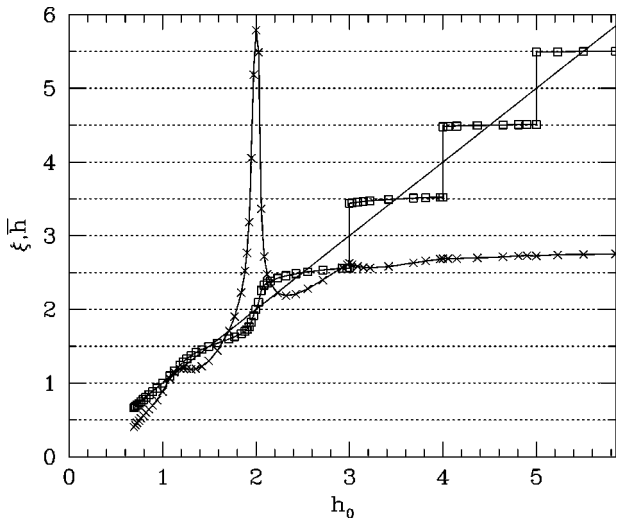

FIG. 6. ξ ($\times$) and $\bar{h}$ ($\square$), as a function of h_0, along the adsorption isotherm $T=0.6$, for $T_{PR}=0.5$. Sharp jumps of $\bar{h}$ between half-integer values signal the crossing of first-order reentrant layering transition lines.

In Fig. 6, the behavior at $T=0.6$ (the DOF phase in the bulk interface) is reported. It is similar to Fig. 4, but now $\bar{h}$ and $(\partial\Delta f_{\rm best}/\partial\Delta\mu)_\beta$ jump between half-integer values every time h_0 is an integer. This is the adsorbed film remnant of the DOF phase. As before, ξ shows a cusp whenever $\bar{h}$ jumps, and increases eventually until the bulk value 2.7797. Starting from $h_0=2$, integer values of h_0 define first-order transition lines starting at temperatures $T^{(2)},T^{(3)},T^{(4)},\ldots$, which converge to T_{PR} as a power law, $T^{(n)}-T_{PR}\sim n^{-p_2(T_{PR})}$, with $p_2(T_{PR})\simeq 2.502$. Weichman and Prasad gave a renormalization-group estimate of the same exponent, $p_1(T_{PR})=p_2(T_{PR})=4-[\pi/K_c(T_{PR})]=2.429$,[3] which is encouragingly similar to ours. Finally, the transition lines terminate in noncritical end points at temperatures $T'^{(2)},T'^{(3)},T'^{(4)},\ldots$, which converge to T_R as $T_R-T'^{(n)}\sim(\ln n)^{-r}$, with $r=1.406$ (for comparison, the renormalization-group estimate is $r=2$).[25]

Lastly, we study the behavior at T_{PR} (see Fig. 7). Here both ξ and $\bar{h}$ grow monotonically with h_0, and there is no first-order line ever crossed. To sum up, coming from low temperature, first-order layering transitions disappear just below T_{PR}, only to reappear soon after. At higher temperature, they disappear again, and for good, when roughening is reached. The ensuing phase diagram is shown in Fig. 8.

Next we study the growth of the adsorbed film under conditions where the bulk PR is first order ($T_{PR}<T_R/4$). We use $T_{PR}=0.25$, $C=0.5J$, and $y_4=0.1J$ (see Fig. 2 for the behavior at the bulk interface). A typical low-temperature adsorption isotherm is plotted in Fig. 9 ($T=0.2$). The main difference with respect to Fig. 4 is in the supplementary step around $h_0=1.5$, which is found in the $\bar{h}$ staircase [and in $(\partial\Delta f_{\rm best}/\partial\Delta\mu)_\beta$ as well], signalling a more complex behavior than before. A more accurate analysis shows that the two additional first-order points actually belong to new transition lines, one of which (and precisely that at lower h_0, line A) bifurcates at $T\simeq 0.238$ into two first-order lines (one ending at $T\simeq 0.269$ with vanishing $\bar{h}$ jump, and the other at

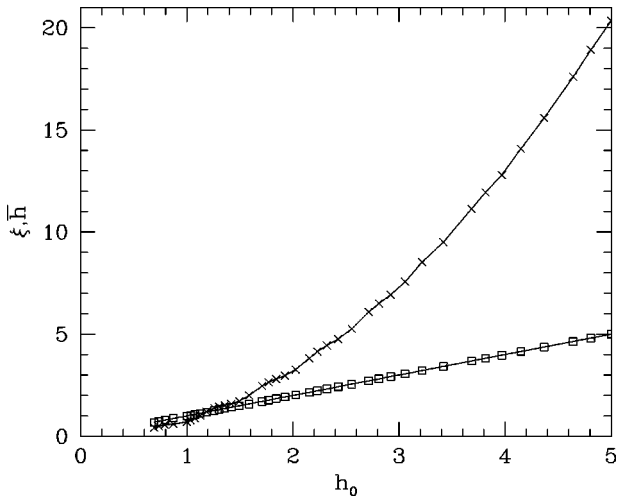

FIG. 7. ξ ($\times$) and $\bar{h}$ ($\square$), as a function of h_0, along the adsorption isotherm $T=T_{PR}=0.5$. The correlation length increases to infinity as $\Delta\mu\to 0$, and no transition line is ever crossed.

$T\simeq 0.273$) enclosing a region where $\bar{h}\simeq 1.25$. The other transition line (B) joins the first reentrant line on the DOF side of the phase diagram (see below in this section) at $T=0.2919$. Other details are similar to the $T_{PR}=0.5$ case: ξ has a cusp at every $\bar{h}$ jump, growing eventually until the bulk value 0.4978; the first-order lines at $h_0=1.5,2.5,3.5,\ldots$ terminate in noncritical end points, whose temperatures $T^{(1.5)},T^{(2.5)},T^{(3.5)},\ldots$ converge to T_{PR} as a power law, $T_{PR}-T^{[n-(1/2)]}\sim n^{-q_1}$, with $q_1\simeq 4.405$.

The phase with coverage $\bar{h}\simeq 1.25$ is an unexpected realization of Den Nijs's θ-DOF phase,[26,19] in the presence of a strong substrate. We now wish to understand how it comes about. It is shown in Appendix A that θ-DOF phase solutions characterized by some fractional coverage $\bar{h}$ generally do exist as local free-energy minima [cf. Eq. (A31)]. Without a

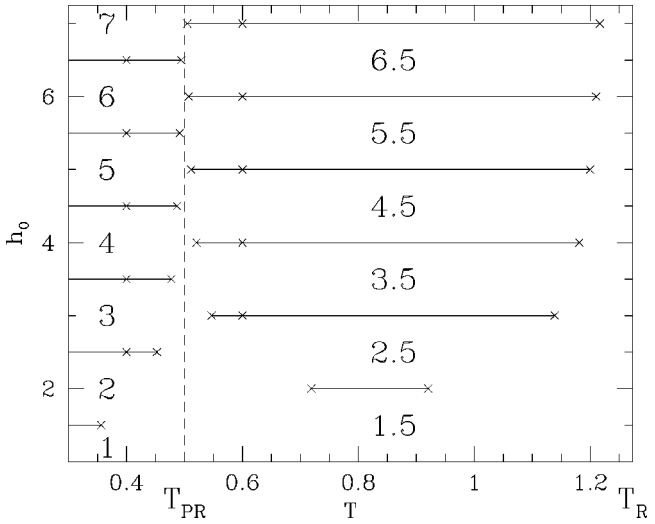

FIG. 8. Phase diagram of the film for $T_{PR}=0.5$, $C=0.5J$, and $y_4=0.1J$. With these parameters, the bulk preroughening is critical. Our data points (including noncritical end points) are marked with an $\times$. The low-temperature layering transition lines are followed, past the preroughening point, by another series of lines which bound phase-diagram regions where the film height is half-integer.

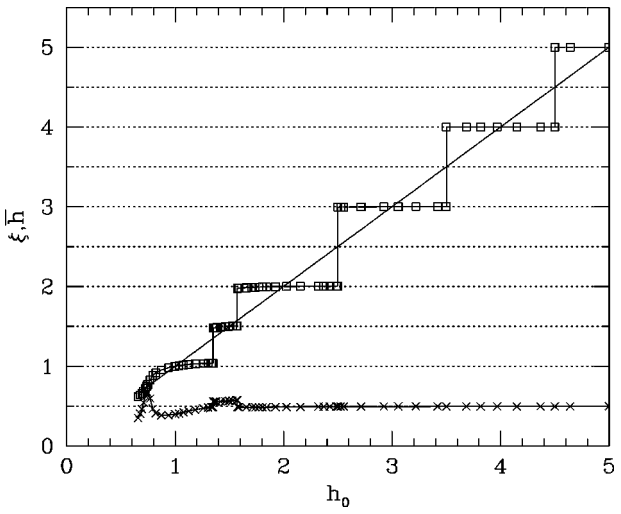

FIG. 9. ξ ($\times$) and $\bar{h}$ ($\square$), as a function of h_0, along the adsorption isotherm $T=0.2$, for $T_{PR}=0.25$. We notice the additional step around 1.5 and the related ξ jumps. Sharp jumps of $\bar{h}$ signal the crossing of first-order layering transition lines.

substrate, however, they can be global minima only if $y_4<0$. This is a rather common circumstance, although models which realize it have only recently been discussed.[19]

What we find here is that a strong attractive substrate and a large correlation length ξ can stabilize a phase $\bar{h}\simeq 1.25$ near PR, even when $y_4>0$. The key factor is that ξ tends to develop maxima at coverage $\bar{h}=(2n+1)/4$. This can be seen directly in Figs. 10 and 11, and understood in Eq. (6.6), for $y_2=0$, $y_4>0$. Since $\cos(4\pi\bar{h})=-1$ at this $\bar{h}$, the last term cancels part of V'', hence ξ becomes large. Given a large ξ and a strong substrate V'', consider, for example, the total free energy (6.4) for $y_2=0$, $y_4>0$, at $h_0=1.25$. We see that $\bar{h}=\frac{5}{4}$ can prevail because the main destabilizing y_4 term is reduced by a large ξ, so that the main stabilizing V'' term (which vanishes only at $\bar{h}=\frac{5}{4}$ but is otherwise positive) can

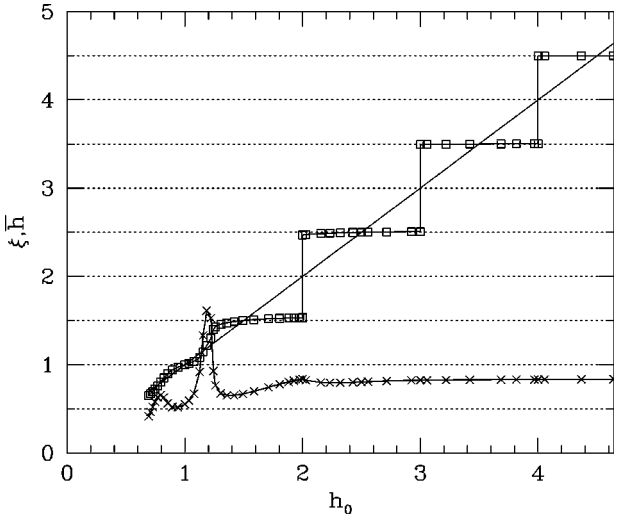

FIG. 10. Same as in Fig. 9, along the adsorption isotherm $T=0.3$, for $T_{PR}=0.25$. The film height jumps between half-integer values, each time a first-order reentrant layering transition line is crossed.

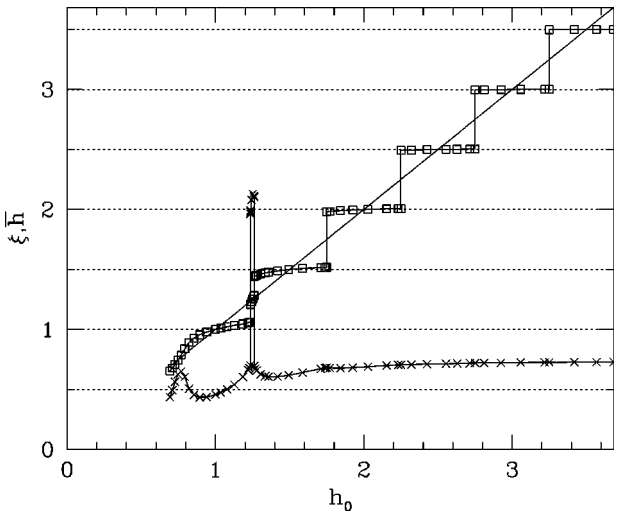

FIG. 11. ξ ($\times$) and $\overline{h}$ ($\square$), as a function of h_0, along the adsorption isotherm $T=T_{PR}=0.25$. We notice the additional $\overline{h}$ step around 1.25 and the related ξ jumps.

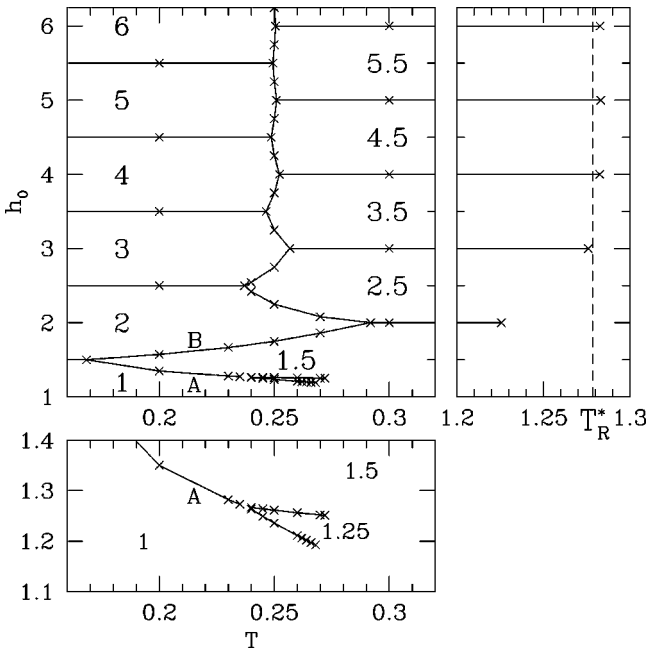

FIG. 12. Phase diagram of the film for $T_{PR}=0.25$, $C=0.5J$, and $y_4=0.1J$. With these parameters, the bulk preroughening is first order. Our data points (including noncritical end points) are marked with an $\times$. We show in more detail in the picture below the additional basin where $\overline{h}\simeq 1.25$. At variance with the phase diagram in Fig. 8, the two series of transition lines are now sewn by a zipper. Similar features are seen in the phase diagram of rare-gas films deposited on graphite (Ref. 9).

take over. A more physical way to rationalize a quarter-coverage θ-DOF phase is to note that close to $(2n+1)/4$ the substrate acts to renormalize the value of y_4, which may become effectively negative.

In Fig. 10 the $T=0.3$ isotherm is shown. A very similar behavior to that of Fig. 6 is found: $\overline{h}$ jumps (and the $\Delta\mu$ derivative of Δf_{best} behaves the same) between half-integer values every time h_0 takes an integer value; correspondingly, ξ has a cusp, while increasing with h_0 up to the bulk value 0.8376. Starting from $h_0=2$, integer values of h_0 define first-order transition lines originating at $T^{(2)},T^{(3)},T^{(4)},\ldots$, which converge to T_{PR} as $T^{(n)}-T_{PR}\sim n^{-q_2}$, with $q_2\simeq 3.802$. Weichman and Prasad gave an estimate of 4 for $q_1=q_2$,[3] which is close to ours. The transition lines survive only below the roughening temperature; they end in noncritical points at $T'^{(2)},T'^{(3)},T'^{(4)},\ldots$, showing a nonmonotonic trend to $T_R^*(0.25)$.

The $T=0.25$ isotherm (Fig. 11) gives a conclusive indication of the overall structure of the film phase diagram when $T_{PR}<T_R/4$. At T_{PR}, there is a radically different behavior than that represented in Fig. 7. Besides the pair of jumps which occur when the fork stemming from line A is crossed, further jumps of $\overline{h}$ are found at $h_0=1.75+(n/2)$ $(n=0,1,2,\ldots)$, the former at the crossing of line B, and the others along the ''zipper'' that joins the $T<T_{PR}$ first-order lines to the $T>T_{PR}$ first-order lines. In the end, the phase diagram of the film looks like Fig. 12.

The ''zippering'' behavior found for $T_{PR}<T_R/4$ is quite similar to the experimental results,[9] as well as to the outcome of renormalization-group theory.[3] In fact, the zipper which is present in the phase diagram of argon films strongly suggests first-order PR of Ar(111). We note that for the Ar(111) surface $T_{PR}=69$ K, $T_R=80$ K, so the condition $T_{PR}<T_R/4$ is far from being verified. We conclude that there must be other physics, not contained in our modeling, and probably not contained in any rigid lattice model, which is at work in making quantitatively the PR of Ar(111) first order.

Finally, we add some remarks on the changes introduced in the foregoing results when including third- and fourth-order terms in the substrate potential. We considered, in particular, the isotherms plotted in Figs. 4 and 11. Actually, only minor changes have to be noted (i.e., no further transition line is found). In both cases, the main quantitative corrections come about, as expected, for low h_0. First of all, $\overline{h}$ jumps will occur at slightly lower h_0 values than before, with appreciable differences only for large $\Delta\mu$. This suggests a small bending downwards of all the transition lines in Figs. 8 and 12. More important, each time a transition line is crossed, the correlation length also makes a jump (while a cusp was seen before). Moreover, the first (and most important) ξ maximum is slightly depleted. Finally, the numerical agreement between $\overline{h}$ and $(\partial\Delta f_{\text{best}}/\partial\Delta\mu)_\beta$ considerably improves, and this provides a successful check of internal consistency of our numerical procedure.

VIII. CONCLUSIONS

In this paper, we have introduced a mean-field variational theory of preroughening (PR) of crystal surfaces, which generalizes previous approaches devoted to roughening.[12,24] We find that many features of both preroughening and roughening are well described in this simple theory. In particular, PR of a rigid lattice model is correctly predicted to be a nonuniversal second-order transition, at least when $T_{PR}>T_R/4$. In this case, the theory connects the critical exponents and the roughness parameter at PR to the ratio of the two temperatures. For T_{PR} below this threshold value, PR is predicted to become first order, in agreement with Ref. 3.

Surface dynamics is also described by the theory. Growth

is continuous at both PR and roughening (when not first order), as well as—of course—in the whole rough phase; in all other cases, the growth mode is layer by layer. In this regime, there is a threshold which the driving force must overcome in order for the crystal to become depinned and start growing, both below and above T_{PR}. This is the direct extension to preroughening of the known result, obtained by Nozières and Gallet[18] in the simple sine-Gordon model, and by Kotrla and Levi in a kinetic solid-on-solid model,[23] that the interface mobility for a finite driving force is enhanced just below the roughening temperature. The behavior of the depinning field close to T_{PR} is critical, with the same exponent ω of the free energy.

Finally, we find that the variational approach can reproduce many of the subtle features of the layering phase diagram of noble gases adsorbed on an attractive substrate. In particular, if parameters are chosen such that bulk PR is first order, clear evidence is found for the zippering behavior observed in the experiments[9] and also predicted by renormalization-group arguments.[3,19] A substrate-induced θ-DOF phase is also predicted, leading to a quarter-coverage region in the phase diagram.

ACKNOWLEDGMENTS

This research was partly sponsored through INFM, PRA/LOTUS, and by the Italian Ministry of University and Research, under COFIN 97.

APPENDIX A: VARIATIONAL FREE ENERGY

In this appendix, we compute some surface quantities which are averages over the ensemble specified by the quadratic Hamiltonian $\mathcal{H}_0$ in Eq. (3.3), with continuous heights. We first simplify the notation by defining a matrix V, such that

$$\frac{\beta J}{2}\sum_{i,\delta}(h_i-h_{i+\delta})^2=\sum_{\mathbf{x},\mathbf{y}}h_{\mathbf{x}}V_{\mathbf{x},\mathbf{y}}h_{\mathbf{y}}\equiv hVh. \tag{A1}$$

We use $\mathbf{x},\mathbf{y},\ldots$, as well as $i,j,\ldots$, throughout this section to indicate the sites of a square lattice. Equation (A1) yields

$$V_{\mathbf{x},\mathbf{y}}=\beta J(4\delta_{\mathbf{x},\mathbf{y}}-\delta_{|\mathbf{x}-\mathbf{y}|,1})=V_{\mathbf{y},\mathbf{x}}. \tag{A2}$$

Translational invariance of V imposes the existence of plane-wave eigenvectors

$$\sum_{\mathbf{y}}V_{\mathbf{x},\mathbf{y}}e^{i\mathbf{p}\cdot\mathbf{y}}=\lambda(\mathbf{p})e^{i\mathbf{p}\cdot\mathbf{x}}, \tag{A3}$$

with eigenvalues

$$\lambda(\mathbf{p})=2\beta J(2-\cos p_x-\cos p_y) \tag{A4}$$

(we choose a unitary horizontal lattice spacing). We use periodic boundary conditions to fix the $\mathbf{p}$ values. For a rectangular $L_x\times L_y$ box, we have $\mathbf{p}=(n_x/L_x)\mathbf{b}_x+(n_y/L_y)\mathbf{b}_y$, with $n_x=0,1,\ldots,L_x-1$, $n_y=0,1,\ldots,L_y-1$, $\mathbf{b}_x=2\pi\mathbf{e}_x$, and $\mathbf{b}_y=2\pi\mathbf{e}_y$.

Using orthogonality of plane waves, Eq. (A3) can be easily solved in $V_{\mathbf{x},\mathbf{y}}$, as

$$V_{\mathbf{x},\mathbf{y}}=\frac{1}{N}\sum_{\mathbf{p}}\lambda(\mathbf{p})e^{i\mathbf{p}\cdot(\mathbf{x}-\mathbf{y})}. \tag{A5}$$

A similar formula gives the inverse-matrix elements

$$V^{-1}_{\mathbf{x},\mathbf{y}}=\frac{1}{N}\sum_{\mathbf{p}}\frac{e^{i\mathbf{p}\cdot(\mathbf{x}-\mathbf{y})}}{\lambda(\mathbf{p})}. \tag{A6}$$

The infrared divergence in Eq. (A6) can be healed up by introducing a small mass term which must eventually be set to zero when evaluating measurable quantities like, for instance, the pair correlations [see Eq. (A11) below].

In order to calculate thermodynamic averages over quadratic Hamiltonians, the Gaussian integral

$$\int \mathcal{D}h\ e^{-hVh+bh}=\pi^{N/2}(\det V)^{-(1/2)}e^{(1/4)bV^{-1}b}, \tag{A7}$$

is useful, where V is any positive-definite matrix, $h=\{\ldots,h_i,\ldots\}$, and b is any complex N-component vector. We used the notation $\mathcal{D}h=\Pi_{\mathbf{x}}dh_{\mathbf{x}}$. Observe that $\det V$ is simply the product of the V eigenvalues (all positive). In particular

$$\int \mathcal{D}h\ e^{-hVh}=\Pi_{\mathbf{p}}\left(\frac{\pi}{\lambda(\mathbf{p})}\right)^{1/2} \tag{A8}$$

is the partition function Z_{CG} of the continuous Gaussian (CG) model, which is rough at any temperature. This can be seen from the expression for the average square height difference:

$$\langle(h_{\mathbf{x}}-h_{\mathbf{y}})^2\rangle_{CG}=\frac{2\int\mathcal{D}h(h_{\mathbf{x}}^2-h_{\mathbf{x}}h_{\mathbf{y}})e^{-hVh}}{\int\mathcal{D}he^{-hVh}}. \tag{A9}$$

Using the result

$$\int \mathcal{D}h\ h_{\mathbf{x}}h_{\mathbf{y}}e^{-hVh}=\left(\frac{\partial^2}{\partial J_{\mathbf{x}}\partial J_{\mathbf{y}}}\int\mathcal{D}h\ e^{-hVh+Jh}\right)_{J=0}$$
$$=\frac{1}{2}Z_{CG}V^{-1}_{\mathbf{x},\mathbf{y}}, \tag{A10}$$

one finally obtains

$$\langle(h_{\mathbf{x}}-h_{\mathbf{y}})^2\rangle_{CG}=\frac{1}{N}\sum_{\mathbf{p}}\frac{1-e^{i\mathbf{p}\cdot(\mathbf{x}-\mathbf{y})}}{\lambda(\mathbf{p})}\sim\frac{1}{2\pi\beta J}\ln|\mathbf{x}-\mathbf{y}|, \tag{A11}$$

which diverges at large distance, although as slow as a logarithm.

Another matrix we introduce is W, defined through

$$\frac{\beta J}{2}\sum_{i,\delta}(h_i-h_{i+\delta})^2+\beta J\xi^{-2}\sum_i h_i^2\equiv hWh. \tag{A12}$$

It is fairly simple to show that

$$W_{\mathbf{x},\mathbf{y}}=\beta J[(4+\xi^{-2})\delta_{\mathbf{x}\mathbf{y}}-\delta_{|\mathbf{x}-\mathbf{y}|,1}] \tag{A13}$$

and

$$\sum_{\mathbf{y}}W_{\mathbf{x},\mathbf{y}}e^{i\mathbf{p}\cdot\mathbf{y}}=g(\mathbf{p})e^{i\mathbf{p}\cdot\mathbf{x}}, \tag{A14}$$

with

$$g(\mathbf{p})=2\beta J\left(2-\cos p_x-\cos p_y+\frac{\xi^{-2}}{2}\right). \tag{A15}$$

At variance with $\lambda(\mathbf{p})^{-1}$,$g(\mathbf{p})^{-1}$ acquires a mass term ξ^{-2} in the large-N long-wavelength limit

$$\beta J g(\mathbf{p})^{-1}\approx\frac{1}{p^2+\xi^{-2}}. \tag{A16}$$

The outcome of this is that a term like $J\xi^{-2}\Sigma_i h_i^2$ in the Hamiltonian makes the surface flat, since it gains a finite correlation length ξ. This follows from the estimate of the average square height difference at large distance, $|\mathbf{x}-\mathbf{y}|\gg\xi$,[12]

$$\langle(h_{\mathbf{x}}-h_{\mathbf{y}})^2\rangle_0=\frac{1}{N}\sum_{\mathbf{p}}\ \frac{1-e^{i\mathbf{p}\cdot(\mathbf{x}-\mathbf{y})}}{g(\mathbf{p})}$$
$$\sim\frac{1}{2\pi\beta J}\left(\ln\xi-\sqrt{\frac{\pi\xi}{2|\mathbf{x}-\mathbf{y}|}}\,e^{-(|\mathbf{x}-\mathbf{y}|/\xi)}\right). \tag{A17}$$

Given all of the above, we calculate the right-hand side of Eq. (3.4). The first ingredient we need is

$$\beta F_0=-\tfrac{1}{2}\sum_{\mathbf{p}}\ \ln[\pi g(\mathbf{p})^{-1}]. \tag{A18}$$

Then, using $h_i'=h_i-\overline{h}$, we have

$$\beta(\mathcal{H}-\mathcal{H}_0)=hVh-h'Wh'+\beta y_2\sum_i\ [1-\cos(2\pi h_i)]$$
$$+\beta y_4\sum_i\ [1-\cos(4\pi h_i)]. \tag{A19}$$

The average of the first part of Eq. (A19), given the formula $\Sigma_{\mathbf{y}}V_{\mathbf{x},\mathbf{y}}=0$ and using Eq. (A10), comes out as

$$\langle hVh-h'Wh'\rangle_0=\langle h'(V-W)h'\rangle_0=\sum_{\mathbf{x},\mathbf{y}}\ (V_{\mathbf{x},\mathbf{y}}-W_{\mathbf{x},\mathbf{y}})$$
$$\times\langle h_{\mathbf{x}}'h_{\mathbf{y}}'\rangle_0=\tfrac{1}{2}\sum_{\mathbf{x},\mathbf{y}}\ (V_{\mathbf{x},\mathbf{y}}-W_{\mathbf{x},\mathbf{y}})W^{-1}_{\mathbf{x},\mathbf{y}}$$
$$=\tfrac{1}{2}\sum_{\mathbf{p}}\ [g(\mathbf{p})^{-1}\lambda(\mathbf{p})-1]. \tag{A20}$$

Then it follows from Eq. (A7) that

$$\langle e^{ibh}\rangle_0=e^{ib\overline{h}}e^{-(1/4)bW^{-1}b}, \tag{A21}$$

with $b\overline{h}=\overline{h}\Sigma_i b_i$. In particular:

$$\langle e^{\pm 2\pi i h_{\mathbf{x}}}\rangle_0=e^{\pm 2\pi i\overline{h}}e^{-(\pi^2/N)\Sigma_{\mathbf{p}}g(\mathbf{p})^{-1}}. \tag{A22}$$

Collecting together all the foregoing results, we finally obtain

$$\beta F^*\equiv\beta F_0+\beta\langle\mathcal{H}-\mathcal{H}_0\rangle_0=-\tfrac{1}{2}\sum_{\mathbf{p}}\ \ln[\pi g(\mathbf{p})^{-1}]+\tfrac{1}{2}\sum_{\mathbf{p}}\ [g(\mathbf{p})^{-1}\lambda(\mathbf{p})-1]+N\beta y_2$$
$$\times\left[1-\cos(2\pi\overline{h})\exp\left(-\frac{\pi^2}{N}\sum_{\mathbf{p}}\ g(\mathbf{p})^{-1}\right)\right]+N\beta y_4\left[1-\cos(4\pi\overline{h})\exp\left(-\frac{4\pi^2}{N}\sum_{\mathbf{p}}\ g(\mathbf{p})^{-1}\right)\right]. \tag{A23}$$

Choosing $g(\mathbf{p})$ and $\overline{h}=\langle h_i\rangle_0$ as free parameters, we select them by requiring that βF^* be minimum. A necessary condition for that is to have $\delta F^*=0$, from which

$$g(\mathbf{p})=\lambda(\mathbf{p})+2\pi^2\beta y_2\cos(2\pi\overline{h})\exp\left(-\frac{\pi^2}{N}\sum_{\mathbf{p}}\ g(\mathbf{p})^{-1}\right)+8\pi^2\beta y_4\cos(4\pi\overline{h})\exp\left(-\frac{4\pi^2}{N}\sum_{\mathbf{p}}\ g(\mathbf{p})^{-1}\right) \tag{A24}$$

and

$$\sin(2\pi\overline{h})\left[y_2+4y_4\cos(2\pi\overline{h})\exp\left(-\frac{3\pi^2}{N}\sum_{\mathbf{p}}\ g(\mathbf{p})^{-1}\right)\right]=0. \tag{A25}$$

Among the solutions to the two joint equations (A24) and (A25), we must ultimately choose the one providing the absolute minimum of βF^*. In turn, this gives those $\overline{h}(T)$ and $\xi(T)$ that qualify the thermodynamic phases of the surface as described by the Hamiltonian (3.1).

We can further simplify Eqs. (A24) and (A25) by making explicit the ξ dependence. In the thermodynamic limit, a sum $\Sigma_{\mathbf{p}}F(p)$ is evaluated as $N\int_{BZ}[d\mathbf{p}/(2\pi)^2]F(p)\approx(N/2\pi)\int_0^\pi pF(p)dp$. We thus find

$$-\tfrac{1}{2}\sum_{\mathbf{p}}\ \ln[\pi g(\mathbf{p})^{-1}]$$
$$=-\frac{N}{8}\pi\ln\frac{\pi}{\beta J}+\frac{N}{8\pi}(\pi^2+\xi^{-2})$$
$$\times\ln(\pi^2+\xi^{-2})+\frac{N}{4\pi}\xi^{-2}\ln\xi-\frac{N}{8}\pi, \tag{A26}$$

$$\tfrac{1}{2}\sum_{\mathbf{p}}\left[g(\mathbf{p})^{-1}\lambda(\mathbf{p})-1\right]=-\frac{N}{8\pi}\xi^{-2}\ln[1+(\pi\xi)^2], \tag{A27}$$

$$\exp\left(-\frac{\pi^2}{N}\sum_{\mathbf{p}} g(\mathbf{p})^{-1}\right)=[1+(\pi\xi)^2]^{-(\pi/4\beta J)}. \tag{A28}$$

In particular, βF^* in the rough phase is given by:

$$\beta F^*(\xi^{-2}=0)=-\frac{N}{8}\pi\ln\frac{\pi}{\beta J}+\frac{N}{8}\pi[\ln(\pi^2)-1] +N\beta(y_2+y_4). \tag{A29}$$

Choosing the free energy of the rough surface as the reference, we have

$$\begin{aligned}\beta\Delta f^*&\equiv\frac{1}{N}[\beta F^*-\beta F^*(\xi^{-2}=0)]\\ &=\frac{\pi}{8}\ln[1+(\pi\xi)^{-2}]\\ &\quad-\beta y_2\cos(2\pi\bar{h})[1+(\pi\xi)^2]^{-(\pi/4\beta J)}\\ &\quad-\beta y_4\cos(4\pi\bar{h})[1+(\pi\xi)^2]^{-(\pi/\beta J)}.\end{aligned} \tag{A30}$$

From Eq. (A25), we obtain three possible choices for $\bar{h}$:

$$\begin{aligned}&(1)\quad \bar{h}=\ldots,-2,-1,0,1,2,\ldots,\\ &(2)\quad \bar{h}=\ldots,-\tfrac{3}{2},-\tfrac{1}{2},\tfrac{1}{2},\tfrac{3}{2},\ldots,\\ &(3)\quad \cos(2\pi\bar{h})=-\frac{y_2}{4y_4}[1+(\pi\xi)^2]^{3\pi/4\beta J}.\end{aligned} \tag{A31}$$

Solutions of type (1) correspond to the ordered flat surface, and those of type (2) to the disordered flat (DOF) surface. Type (3), finally, corresponds to the so-called θ-DOF surface.[26,3,19] In particular, a necessary condition for solutions of type (3) to be valid is $\xi\leqslant 1/\pi[(4y_4/|y_2|)^{4\beta J/3\pi}-1]^{1/2}$. Plugging Eq. (A31) into Eq. (A30), we obtain three possible expressions for the free energy:

$$\begin{aligned}\beta\Delta f_1^*&=\frac{\pi}{8}\ln[1+(\pi\xi)^{-2}]-\beta y_2[1+(\pi\xi)^2]^{-(\pi/4\beta J)}\\ &\quad-\beta y_4[1+(\pi\xi)^2]^{-\pi/\beta J},\\ \beta\Delta f_2^*&=\frac{\pi}{8}\ln[1+(\pi\xi)^{-2}]+\beta y_2[1+(\pi\xi)^2]^{-(\pi/4\beta J)}\\ &\quad-\beta y_4[1+(\pi\xi)^2]^{-(\pi/\beta J)},\\ \beta\Delta f_3^*&=\frac{\pi}{8}\ln[1+(\pi\xi)^{-2}]+\frac{\beta y_2^2}{8y_4}[1+(\pi\xi)^2]^{\pi/2\beta J}\\ &\quad+\beta y_4[1+(\pi\xi)^2]^{-(\pi/\beta J)}.\end{aligned} \tag{A32}$$

We immediately see that free energy of type (3), when it does exist, is always larger than the other two, so long as $y_4>0$. This is no longer true when $y_4<0$, where stable θ-DOF phases can appear.[3,19] Even for $y_4>0$, solution type (3) may become relevant in presence of a strong substrate (see Sec. VII). For a free surface, and with $y_4>0$, we can ignore this, and the ξ functional to minimize becomes

$$\begin{aligned}\beta\Delta f^*&=\frac{\pi}{8}\ln[1+(\pi\xi)^{-2}]-\beta|y_2|[1+(\pi\xi)^2]^{-(\pi/4\beta J)}\\ &\quad-\beta y_4[1+(\pi\xi)^2]^{-(\pi/\beta J)},\end{aligned} \tag{A33}$$

with $\bar{h}$ being an integer for $T<T_{PR}$ and a half-integer for $T>T_{PR}$. Similarly, Eq. (A24) can be rewritten as

$$\begin{aligned}J\xi^{-2}&=2\pi^2|y_2|[1+(\pi\xi)^2]^{-(\pi/4\beta J)}\\ &\quad+8\pi^2 y_4[1+(\pi\xi)^2]^{-(\pi/\beta J)}.\end{aligned} \tag{A34}$$

Minimization of the variational free energy (A33) is discussed in Sec. III, together with the analysis of the solutions to Eq. (A34).

Our final comment is about the lattice geometry. One may ask whether the above conclusions retain their validity if a different host lattice is used. In particular, here we consider here the case of a triangular lattice. We expect that only nonuniversal quantities like the transition temperatures depend upon the lattice geometry. In order to prove this, we start from Eqs. (A2) and (A4). In the hypothesis of a triangular host lattice, they are to be modified as follows:

$$V_{\mathbf{x},\mathbf{y}}=\beta J(6\delta_{\mathbf{x},\mathbf{y}}-\delta_{|\mathbf{x}-\mathbf{y}|,1}) \tag{A35}$$

and

$$\begin{aligned}\lambda(\mathbf{p})&=2\beta J\left[3-\cos p_x-\cos\left(\frac{p_x+\sqrt{3}p_y}{2}\right)-\cos\left(\frac{p_x-\sqrt{3}p_y}{2}\right)\right]\\ &\approx\frac{3}{2}\beta J p^2,\end{aligned} \tag{A36}$$

respectively. Similarly, Eq. (A16) becomes

$$\beta J g(\mathbf{p})^{-1}\approx\frac{1}{\frac{3}{2}p^2+\xi^{-2}}, \tag{A37}$$

with different wave vectors than before. They now read $\mathbf{p}=(n_x/L_x)\mathbf{b}_x+(n_y/L_y)\mathbf{b}_y$, with $\mathbf{b}_x=2\pi[\mathbf{e}_x-(1/\sqrt{3})\mathbf{e}_y]$ and $\mathbf{b}_y=(4\pi/\sqrt{3})\mathbf{e}_y$. In particular, the area of the first Brillouin zone is now $(2\pi\sqrt{2/\sqrt{3}})^2$, and the rule for summing up over all wave vectors becomes:

$$\begin{aligned}\frac{1}{N}\sum_{\mathbf{p}}F(p)&\simeq\frac{\sqrt{3}}{2}\int_{BZ}\frac{d\mathbf{p}}{(2\pi)^2}F(p)\approx\frac{\sqrt{3}}{4\pi}\int_0^{\sqrt{2/\sqrt{3}}\pi}pF(p)dp\\ &=\frac{1}{2\pi}\int_0^{\pi}p'F\left(\sqrt{\frac{2}{\sqrt{3}}}p'\right)dp'.\end{aligned} \tag{A38}$$

Given Eq. (A38), and defining $J'=\sqrt{3}J$, $\xi'^{-2}=\xi^{-2}/\sqrt{3}$, we see that any expression involving only sums of $g(\mathbf{p})$ functionals, like the free energy (A23), becomes equivalent to its square-lattice form if we just replace J with J' and ξ with ξ'. In this way, the theory exposed above is still valid [with the only exception of Eq. (A17), to which Eq. (A38) is not directly applicable], but with a new temperature scale (J'/k_B instead of J/k_B) and also a rescaled correlation length. In

particular, surface roughening on the triangular lattice would occur at $4\sqrt{3}/\pi$ (in units of J/k_B).

APPENDIX B: FOKKER-PLANCK EQUATION

This appendix is meant to help the reader follow our derivation, which is formally somewhat different from that of Saito,[12] even if close in its essence. We derive differential equations for the average height and the pair-correlation function in nonequilibrium conditions when a Gaussian ansatz is made on the height distribution function $P(\{h_i\},t)$, abbreviated as $P(h,t)$. The latter obeys the Fokker-Planck equation (5.5), which we here reproduce for the reader's convenience:

$$\frac{\partial P(h,t)}{\partial t}=\frac{\beta}{\tau}\sum_i \frac{\delta}{\delta h_i}\left(P\frac{\delta\mathcal{H}}{\delta h_i}+\frac{1}{\beta}\frac{\delta P}{\delta h_i}\right). \tag{B1}$$

Here $\mathcal{H}$ contains a term $-\Delta\mu\Sigma_i h_i$ which makes the crystal grow at the expense of the vacuum. Note that the stationary solution to Eq. (B1) for $\Delta\mu=0$ is $P_{\rm eq}(h)\propto\exp(-\beta\mathcal{H})$, which ensures Boltzmann fluctuations at equilibrium.

We denote as $\langle\cdots\rangle_P$ the average $\int\mathcal{D}h\ P(h,t)(\cdots)$ over the height distribution. First we calculate the evolution of the height at a given site of the lattice:

$$\frac{d}{dt}\langle h_i\rangle_P=\int\mathcal{D}h\ \frac{\partial P(h,t)}{\partial t}h_i=-\frac{\beta}{\tau}\int\mathcal{D}h\left(P\frac{\delta\mathcal{H}}{\delta h_i}+\frac{1}{\beta}\frac{\delta P}{\delta h_i}\right)$$
$$=-\frac{\beta}{\tau}\left\langle\frac{\delta\mathcal{H}}{\delta h_i}\right\rangle_P, \tag{B2}$$

where we used the fact that P goes to zero at infinity. Then, we consider the second cumulant $\langle\!\langle(h_i-\langle h_i\rangle_P)(h_j-\langle h_j\rangle_P)\rangle\!\rangle_P$, whose first-order time derivative reads

$$\int\mathcal{D}h\ \frac{\partial P(h,t)}{\partial t}(h_i-\langle h_i\rangle_P)(h_j-\langle h_j\rangle_P)=-\frac{\beta}{\tau}\left[\int\mathcal{D}h\left(P\frac{\delta\mathcal{H}}{\delta h_i}+\frac{1}{\beta}\frac{\delta P}{\delta h_i}\right)(h_j-\langle h_j\rangle_P)+\int\mathcal{D}h\left(P\frac{\delta\mathcal{H}}{\delta h_j}+\frac{1}{\beta}\frac{\delta P}{\delta h_j}\right)(h_i-\langle h_i\rangle_P)\right]$$
$$=-\frac{\beta}{\tau}\left[\left\langle\frac{\delta\mathcal{H}}{\delta h_i}(h_j-\langle h_j\rangle_P)\right\rangle_P+\left\langle\frac{\delta\mathcal{H}}{\delta h_j}(h_i-\langle h_i\rangle_P)\right\rangle_P-\frac{2}{\beta}\delta_{ij}\right]. \tag{B3}$$

Equations (B2) and (B3) are to be made explicit by specifying the form of P. We make two assumptions.[12] (1) homogeneity, $\langle h_i\rangle_P=\overline{h}(t)$; and (2) Gaussian distribution for the heights, i.e., $P(h,t)\propto\exp\{-\Sigma_{i,j}[h_i-\overline{h}(t)]W_{ij}(t)[h_j-\overline{h}(t)]\}$, with $W_{ij}=W_{ji}=W_{i+k,j+k}$. This last assumption is not bad, provided the system is not much far from equilibrium. Using

$$\frac{\delta\mathcal{H}}{\delta h_i}=2J\sum_\delta\ (h_i-h_{i+\delta})+2\pi y_2\sin(2\pi h_i)+4\pi y_4\sin(4\pi h_i)-\Delta\mu, \tag{B4}$$

we readily obtain

$$\frac{d\overline{h}(t)}{dt}=\frac{\beta}{\tau}\left[\Delta\mu-2\pi y_2\sin[2\pi\overline{h}(t)]\exp\left(-\frac{\pi^2}{N}\sum_{\mathbf{p}}\ g(\mathbf{p},t)^{-1}\right)-4\pi y_4\sin[4\pi\overline{h}(t)]\exp\left(-(4\pi^2/N)\sum_{\mathbf{p}}\ g(\mathbf{p},t)^{-1}\right)\right], \tag{B5}$$

where the following resolution was used:

$$W^{-1}_{\mathbf{xy}}(t)=\frac{1}{N}\sum_{\mathbf{p}}\ \frac{e^{i\mathbf{p}\cdot(\mathbf{x}-\mathbf{y})}}{g(\mathbf{p},t)}. \tag{B6}$$

Note that in the absence of any driving force the system gradually approaches equilibrium, and Eq. (B5) gives back Eq. (A25).

Then we need the evolution equation of $g(\mathbf{p},t)$. To this end, we use Eq. (B3) which we now make less cumbersome. First, we have [cf. Eq. (A10)]

$$\langle[h_i-\overline{h}(t)][h_j-\overline{h}(t)]\rangle_P=\tfrac{1}{2}W^{-1}_{ij}(t). \tag{B7}$$

Upon inserting Eq. (B4) into Eq. (B3), we are led to evaluate $\langle[h_i-\overline{h}(t)]\sin(2\pi h_j)\rangle_P$. Using the same trick as in Eq. (A10), we obtain

$$\langle[h_i-\overline{h}(t)]e^{\pm 2\pi i h_j}\rangle_P=\pm\pi i W^{-1}_{ij}e^{\pm 2\pi i\overline{h}(t)}\times\exp\left(-\frac{\pi^2}{N}\sum_{\mathbf{p}}\ g(\mathbf{p},t)^{-1}\right), \tag{B8}$$

and finally

$$\langle[h_i-\overline{h}(t)]\sin(2\pi h_j)\rangle_P=\pi W^{-1}_{ij}\cos[2\pi\overline{h}(t)]\times\exp\left(-\frac{\pi^2}{N}\sum_{\mathbf{p}}\ g(\mathbf{p},t)^{-1}\right). \tag{B9}$$

Likewise, we have

$$\langle [h_i-\overline{h}(t)]\sin(4\pi h_j)\rangle_P = 2\pi W_{ij}^{-1}\cos[4\pi\overline{h}(t)] \times\exp\left(-\frac{4\pi^2}{N}\sum_{\mathbf{p}} g(\mathbf{p},t)^{-1}\right). \tag{B10}$$

Finally, using Eqs. (B7) and (A4), we obtain

$$\left\langle \sum_{\delta} (h_i-h_{i+\delta})[h_j-\overline{h}(t)]\right\rangle_P = \frac{1}{2}\sum_{\delta}(W_{ij}^{-1}-W_{i+\delta,j}^{-1}) = \frac{1}{2\beta J}\lambda(\mathbf{p})W_{ij}^{-1}. \tag{B11}$$

Collecting together all partial results, and using $\delta_{\mathbf{xy}} = (1/N)\Sigma_{\mathbf{p}} e^{i\mathbf{p}\cdot(\mathbf{x}-\mathbf{y})}$, we find, in the end

$$\frac{d}{dt}g(\mathbf{p},t)^{-1} = -\frac{4}{\tau}g(\mathbf{p},t)^{-1} \times\Big[\lambda(\mathbf{p})-g(\mathbf{p},t)+2\pi^2\beta y_2\cos[2\pi\overline{h}(t)] \times\exp\left(-\frac{\pi^2}{N}\sum_{\mathbf{p}} g(\mathbf{p},t)^{-1}\right) +8\pi^2\beta y_4\cos[4\pi\overline{h}(t)] \times\exp\left(-\frac{4\pi^2}{N}\sum_{\mathbf{p}} g(\mathbf{p},t)^{-1}\right)\Big]. \tag{B12}$$

Again, in stationary conditions, Eq. (B12) gives back the equilibrium result (A24).

*Electronic address: prestip@vulcano.unime.it; tosatti@sissa.it

[1] M. den Nijs and K. Rommelse, Phys. Rev. B **40**, 4709 (1989).
[2] M. den Nijs, Phys. Rev. B **46**, 10 386 (1992).
[3] P. B. Weichman and A. Prasad, Phys. Rev. Lett. **76**, 2322 (1996).
[4] S. Prestipino, G. Santoro, and E. Tosatti, Phys. Rev. Lett. **75**, 4468 (1995).
[5] S. Prestipino, C. S. Jayanthi, F. Ercolessi, and E. Tosatti, Surf. Rev. Lett. **4**, 843 (1997).
[6] G. Santoro, A. Laio, and E. Tosatti, Surf. Sci. (to be published).
[7] S. Prestipino and E. Tosatti, Phys. Rev. B **57**, 10 157 (1998).
[8] H. S. Youn and G. B. Hess, Phys. Rev. Lett. **64**, 918 (1990); P. Day, M. LaMadrid, M. Lysek, and D. Goodstein, Phys. Rev. B **47**, 7501 (1993); H. S. Youn, X. F. Meng, and G. B. Hess, *ibid.* **48**, 14 556 (1993).
[9] P. Day, M. Lysek, M. LaMadrid, and D. Goodstein, Phys. Rev. B **47**, 10 716 (1993).
[10] M. Den Nijs, in *Phase Transitions in Surface Films 2*, edited by H. Taub *et al.* (Plenum, New York, 1992).
[11] F. Celestini, D. Passerone, F. Ercolessi, and E. Tosatti, Surf. Sci. (to be published); and (unpublished).
[12] Y. Saito, Z. Phys. B **32**, 75 (1978).
[13] See, for example, J. D. Weeks, in *Ordering in Strongly Fluctuating Condensed Matter Systems*, edited by T. Riste (Plenum, New York, 1980).
[14] S. T. Chui and J. D. Weeks, Phys. Rev. B **14**, 4978 (1976).
[15] T. Ohta and K. Kawasaki, Prog. Theor. Phys. **60**, 365 (1978).
[16] For a review, see H. Van Beijeren and I. Nolden, in *Structure and Dynamics of Surfaces II: Phenomena, Models and Methods*, edited by W. Schommers and P. Von Blanckenhagen (Springer, Berlin, 1987).
[17] S. T. Chui and J. D. Weeks, Phys. Rev. Lett. **40**, 733 (1978).
[18] P. Nozières and F. Gallet, J. Phys. (Paris) **48**, 353 (1987).
[19] A. Prasad and P. B. Weichman, Phys. Rev. B **57**, 4900 (1998).
[20] See, for example, H. B. Callen, *Thermodynamics and an Introduction to Thermostatistics* (Wiley, New York, 1985), Chap. 20; R. F. Peierls, Phys. Rev. **54**, 918 (1958).
[21] P. J. M. Bastiaansen and H. J. F. Knops, Phys. Rev. B **53**, 126 (1996).
[22] See, for example, N. Goldenfeld, *Lectures on Phase Transitions and the Renormalization Group* (Addison-Wesley, Reading, MA, 1992), Chap. 8.
[23] M. Kotrla and A. C. Levi, Surf. Sci. **317**, 183 (1994).
[24] J. D. Weeks, Phys. Rev. B **26**, 3998 (1982).
[25] D. Huse, Phys. Rev. B **30**, 1371 (1984).
[26] M. den Nijs, Phys. Rev. Lett. **64**, 435 (1990).